

Analysis of one-way laser ranging data to LRO, time transfer and clock characterization

Bauer, S.; Hussmann, H.; Oberst, J.; Dirkx, D.; Mao, D.; Neumann, G. A.; Mazarico, E.; Torrence, M. H.; McGarry, J. F.; Smith, D. E.

DOI

[10.1016/j.icarus.2016.09.026](https://doi.org/10.1016/j.icarus.2016.09.026)

Publication date

2017

Document Version

Final published version

Published in

Icarus

Citation (APA)

Bauer, S., Hussmann, H., Oberst, J., Dirkx, D., Mao, D., Neumann, G. A., Mazarico, E., Torrence, M. H., McGarry, J. F., Smith, D. E., & Zuber, M. T. (2017). Analysis of one-way laser ranging data to LRO, time transfer and clock characterization. *Icarus*, 283, 38-54. <https://doi.org/10.1016/j.icarus.2016.09.026>

Important note

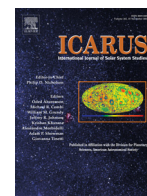
To cite this publication, please use the final published version (if applicable).
Please check the document version above.

Copyright

Other than for strictly personal use, it is not permitted to download, forward or distribute the text or part of it, without the consent of the author(s) and/or copyright holder(s), unless the work is under an open content license such as Creative Commons.

Takedown policy

Please contact us and provide details if you believe this document breaches copyrights.
We will remove access to the work immediately and investigate your claim.



Analysis of one-way laser ranging data to LRO, time transfer and clock characterization



S. Bauer^{a,*}, H. Hussmann^a, J. Oberst^{a,b,c}, D. Dirkx^{d,e}, D. Mao^f, G.A. Neumann^g, E. Mazarico^g, M.H. Torrence^h, J.F. McGarry^g, D.E. Smithⁱ, M.T. Zuberⁱ

^a German Aerospace Center (DLR), Berlin, Germany

^b TU Berlin, Germany

^c Moscow State University for Geodesy and Cartography (MIIGAiK), Russia

^d TU Delft, Netherlands

^e Joint institute for VLBI ERIC, Dwingeloo, Netherlands

^f Sigma Space Corporation, Lanham, MD, USA

^g NASA Goddard Space Flight Center, Greenbelt, MD, USA

^h Stinger Ghaffarian Technologies Inc., Greenbelt, MD, USA

ⁱ Massachusetts Institute of Technology, Cambridge, MA, USA

ARTICLE INFO

Article history:

Received 3 September 2015

Revised 29 July 2016

Accepted 19 September 2016

Available online 21 September 2016

Keywords:

Laser ranging

One-way

Lunar Reconnaissance Orbiter

time transfer

ABSTRACT

We processed and analyzed one-way laser ranging data from International Laser Ranging Service ground stations to NASA's Lunar Reconnaissance Orbiter (LRO), obtained from June 13, 2009 until September 30, 2014.

We pair and analyze the one-way range observables from station laser fire and spacecraft laser arrival times by using nominal LRO orbit models based on the GRAIL gravity field. We apply corrections for instrument range walk, as well as for atmospheric and relativistic effects.

In total we derived a tracking data volume of ≈ 3000 hours featuring 64 million Full Rate and 1.5 million Normal Point observations. From a statistical analysis of the dataset we evaluate the experiment and the ground station performance. We observe a laser ranging measurement precision of 12.3 cm in case of the Full Rate data which surpasses the LOLA timestamp precision of 15 cm. The averaging to Normal Point data further reduces the measurement precision to 5.6 cm.

We characterized the LRO clock with fits throughout the mission time and estimated the rate to 6.9×10^{-8} , the aging to 1.6×10^{-12} /day and the change of aging to 2.3×10^{-14} /day² over all mission phases. The fits also provide referencing of onboard time to the TDB time scale at a precision of 166 ns over two and 256 ns over all mission phases, representing ground to space time transfer. Furthermore we measure ground station clock differences from the fits as well as from simultaneous passes which we use for ground to ground time transfer from common view observations. We observed relative offsets ranging from 33 to 560 ns and relative rates ranging from 2×10^{-13} to 6×10^{-12} between the ground station clocks during selected mission phases. We study the results from the different methods and discuss their applicability for time transfer.

© 2016 Elsevier Inc. All rights reserved.

1. Introduction

NASA's Lunar Reconnaissance Orbiter (LRO) was launched on June 18, 2009 and entered its lunar orbit five days later. The goal of the mission is to carry out a comprehensive geophysical, geological and geochemical mapping campaign to establish an observational framework for future lunar exploration (Zuber et al., 2010).

One of the seven instruments onboard LRO is the Lunar Orbiting Laser Altimeter (LOLA), which was developed at NASA's Goddard Space Flight Center (GSFC), measuring the surface elevation, slope and roughness. From these data a global topographic model and a high-accuracy geodetic grid are derived. LOLA is also capable of detecting laser pulses from Earth ground stations. These one-way range measurements add a new type of tracking data to the mission (Zuber et al., 2010; McGarry et al., 2011 and 2013).

For precise referencing of the orbital remote sensing data, the accuracy and precision of LRO positioning throughout the mission is critical (Zuber et al., 2010). The baseline of the LRO tracking and

* Corresponding author.

E-mail address: sven.bauer@dlr.de (S. Bauer).

orbit determination was realized by radio observations from Earth via NASA's White Sands station and the Universal Space Network (USN) in combination with LOLA's altimetric crossovers. The accuracy of this nominal LRO trajectory which we use in our analysis is reported to be ≈ 9 m overall at the arc overlaps of trajectories consecutive in time (Mazarico et al. 2012 and 2013). Recent solutions of that trajectory used the GRAIL gravity field GRGM900C (Lemoine et al., 2014) up to degree and order 600 (LRO SPICE archive, 2015). The ultimate goal is to combine the various tracking data sets for refined orbit determination to support Lunar precision mapping (Zuber et al., 2010).

Most of the laser ranging experiments beyond an Earth orbit have only been carried out sporadically as for example to Mars Global Surveyor and MESSENGER (Neumann et al., 2006; Smith et al. 2006a). Beside the two-way laser ranging to the mirrors on the lunar surface since the 1970s (Degnan, 1994), only the one-way ranging to LRO has been carried out routinely between June 30, 2009 and September 30, 2014 (McGarry et al. 2013).

Mao et al. (2014a) demonstrated the application of laser ranging data for analysis of the LRO clock and orbit determination. Trajectories derived from various combinations of different types of tracking data were compared in order to assess their consistency. They found that the application of improved gravity fields from the GRAIL mission supports orbit determination with one-way laser ranging data to a quality comparable to radio data based results. Sun et al. (2013a) also used the same laser uplink for demonstration of data transmission which highlights the versatility of the laser ranging to LRO experiment.

Furthermore Sun et al. (2013b) and Mao et al. (2014b) reported about simultaneous passes from multiple stations. They demonstrated the measurement of differences between and the synchronization of remote ground station clocks with the one-way data thus performing ground to ground time transfer. Other optical time transfer experiments like the time transfer by laser link (T2L2) and the European Laser Timing (ELT) have a two-way setup. They derive ground to space and ground to ground time transfer by using an onboard retro-reflector and a detector which provides an active uplink (Exertier et al., 2013; Schreiber et al., 2009).

While previous data analyses have been carried out in the early stages of the experiment (Bauer et al., 2013), we now use all data obtained between July 16, 2009 and September 10, 2014. This report describes the application of the nominal LRO trajectory for the pairing, processing and the analysis of the one-way range measurements as well as the characterization of the onboard clock and the ground station clock differences by time transfer.

We analyze the derived dataset regarding criteria such as pass length, ratio of successfully paired to actually fired shots and measurement precision. From the averaging of these values either over all or all passes of a certain station, we derive the overall and the ground station performance.

Furthermore we use approaches based on the analysis of single and multiple passes in order to characterize the LRO clock by estimating its parameters offset, rate, aging and its change and derive a referencing of onboard to ground time (ground to space time transfer). While we use these terms for the clock parameters they are equivalent to the terms phase, frequency, frequency drift and change of frequency drift respectively, which are used within the time and frequency community. By comparing the parameters derived from the single- and the multiple-pass analysis, we get estimates of their accuracy and precision. We further use the multiple-pass analysis and simultaneous passes to characterize the timing differences between ground station clocks (ground to ground time transfer). Measuring their relative offsets and rates enables the monitoring of their timing.

Section 2 describes the setup and the features of the ground stations that are ranging to LRO along with their timing sys-

tem stabilities. Section 3 provides the setup of the spacecraft and the laser ranging data and discusses the LRO clock stability. Section 4 compares optical two-way time transfer experiments regarding their performance and difference to the time transfer experiment done with the one-way laser ranging data to LRO. Section 5 explains our data processing methods for the pairing, processing and the formation of the Normal Point data as well as the corrections that we apply. In Section 6 we introduce our data analysis methods that utilize either single, multiple or simultaneous passes. The results on the dataset statistics, the characterization of the LRO clock and the ground station clock differences are presented in Section 7. In Section 8 we discuss these results and draw conclusion from our work.

2. Ground stations

LRO is tracked by selected ground stations of the International Laser Ranging Service (ILRS – Pearlman et al., 2002), which differ in their equipment and characteristics as listed in Table 1. Table 2 shows the corresponding stability values of their timing systems. For completion the stability of the LRO onboard clock is added as well, while it is discussed in Section 3 with more detail. With stations in the US, Europe, South Africa (HARL) and Australia (YARL) a global coverage of LRO is basically provided.

Contrary to other established stations, the stations YARL, GODL, MONL and HARL are trailer-based Mobile Laser Ranging Station (MOBLAS). These stations were deployed by NASA in the 1970's for a global tracking of the SEASAT mission (Husson et al., 1992) and have similar hardware and performance characteristics.

3. Spacecraft and data setup

The ranging to LRO as illustrated in Sun et al. (2013a) is done from either one or multiple stations at a time. In order to receive laser shots from Earth ground stations, an optical receiver, the Laser Ranging Telescope was added to the high gain communication antenna which is always pointing towards Earth - in particular, to the White Sands radio station, New Mexico, US, when it is in view. A fiber optic cable is forwarding incoming laser pulses into the LOLA instrument for detection.

From a distance of 381,000 km the Laser Ranging Telescope field of view of 30 mrad covers a circular surface segment with a diameter of $\approx 11,433$ km. With this field of view all US stations to range to LRO simultaneously while the LRO antenna is pointed at White Sands (Ramos et al., 2009).

LOLA has five channels which are designed to receive and detect the 1064 nm lunar return pulses from the laser beams, resulting in five altimetry measurements at a time ideally. The Silicon Avalanche Photodiode (SiAPD) is also able to detect signals at a wavelength of 532 nm (Ramos-Izquierdo et al., 2009), which is commonly used by ILRS ground stations for the ranging to Earth orbiting satellites (Smith et al., 2006b). It is shown in Ramos-Izquierdo et al. (2009) how the signals at both wavelengths are merged. With this setup the regular signals from ILRS Earth ground stations and the returns from the lunar surface can be detected concurrently with the same instrument. Since the LOLA time stamp precision is 0.5 ns, the precision of derived range measurements is ≈ 15 cm.

While the stations record their fire times in UTC, LOLA measures the arrival of laser shots in Mission Elapsed Time (MET), which is the internal timing system of the LRO onboard clock. Within our work we use the Barycentric Dynamical Time (TDB) time scale because it is commonly used for ephemerides and interplanetary orbit determination. Fig. 1 illustrates the relation of these timing systems and their conversion along with the corresponding accuracies. The officially provided data product for the conversion

Table 1
Equipment and characteristics of the ILRS ground stations that range to LRO taken from Mao et al. (2011), McGarry et al. (2011) and the ILRS website (2015).

Code	ID	Location	Coordinates in Lat., Long. and Height	Firing rate in Hz	Synchro-nized firing	Potential received shots per sec	Pulse width in ns	Energy expected at LRO in fJ/cm ²	Type of timing system
MDOL	7080	McDonald, Texas, USA	30.6802° N 104.0152° W 2006 m	10	No	2 to 4	0.20	1 to 10	Cesium
YARL*	7090	Yarragadee, Australia	29.0464° S 115.3467° E 244 m	10	No	2 to 4	0.15	1 to 3	Rubidium
GODL*	7105	Greenbelt, Maryland, USA	39.0206° N 76.8277° W 19 m	10	No	2 to 4	0.15	1 to 3	H-Maser
MONL*	7110	Monument Peak, California, USA	32.8917° N 116.4227° W 1842 m	10	No	2 to 4	0.15	1 to 3	Rubidium
GO1L	7125	Greenbelt, Maryland, USA	39.0206° N 76.8277° W 19 m	28	Yes	28	<8	1 to 5	H-Maser
HARL*	7501	Hartebeesthoek, South Africa	25.8897° S 27.6861° E 1407 m	10	No	2 to 4	0.20	1 to 3	Rubidium
ZIML	7810	Zimmerwald, Switzerland	46.8772° N 7.4652° E 951 m	14	Yes	14	0.06	1 to 3	Oven controlled crystal oscillator
HERL	7840	Herstmonceaux, United Kingdom	50.8674° N 0.3361° E 75 m	14	Yes	14	0.10	1 to 3	H-Maser
GRSM	7845	Grasse, France	43.7546° N 6.9216° E 1323 m	10	No	2 to 4	0.20	1 to 10	Cesium
WETL	8834	Wetzell, Germany	49.1444° N 12.8780° E 665 m	14	Yes	14	0.01	1 to 10	H-Maser

* MOBLAS Stations

Table 2
Stabilities of various ground station timing systems (Lombardi, 2001) and the LRO onboard clock (Cash et al., 2008).

Type	Stability @ noise floor	Averaging period τ in s
Quartz OCXO/OCCO*	1×10^{-12}	1 to 10^2
Rubidium	1×10^{-12}	10^3 to 10^5
Cesium/Atomic	1×10^{-14}	10^5 to 10^7
H-Maser	1×10^{-15}	10^3 to 10^5
LRO onboard clock OCXO*	7×10^{-14}	40

* Oven Controlled Crystal Oscillator

of MET to UTC is the spacecraft clock kernel (SCLK) which has an accuracy of ± 3 ms. Within this work we derive a conversion from

fits (ground to space time transfer) with an accuracy of ± 256 ns over all mission phases (see Sections 6.2 and 7.2).

The LOLA instrument is operating in 28 Hz cycles, which are illustrated in Fig. 2. One major frame with a length of 1 s consists of 28 minor frames with a length of ≈ 35.7 ms each, which include two windows for receiving laser pulses. First, the Earth Range Gate is open for 8 ms, awaiting incoming laser pulses from ground stations. After that the LOLA fires its laser towards the lunar surface ≈ 9.6 ms after t_0 – the beginning of a minor frame. Then, the Lunar Range Gate is open for 5 ms and awaits laser returns from the lunar surface (Riris et al., 2009).

The maximum number of range measurements can be made, when a ground station is firing with frequency and phase matching the LOLA 28 Hz cycle, as it is the case for the GO1L station. For some stations ranging at half of this frequency (e.g. WETL firing

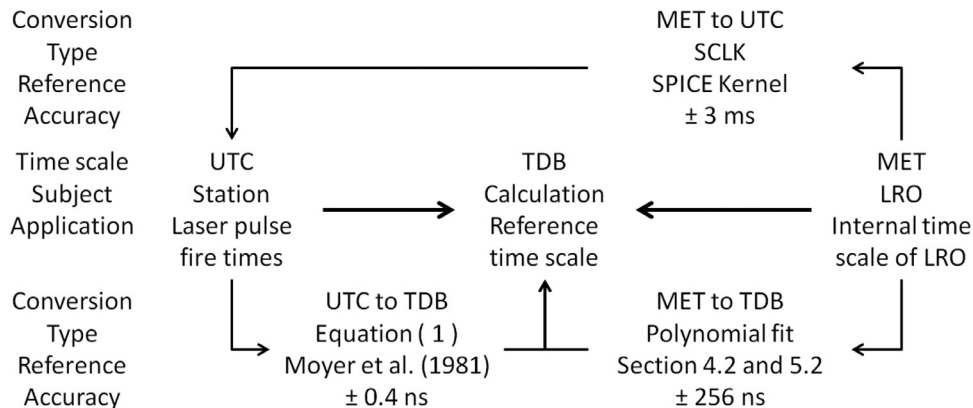


Fig. 1. Utilized time scales with their relation and their conversion accuracies.

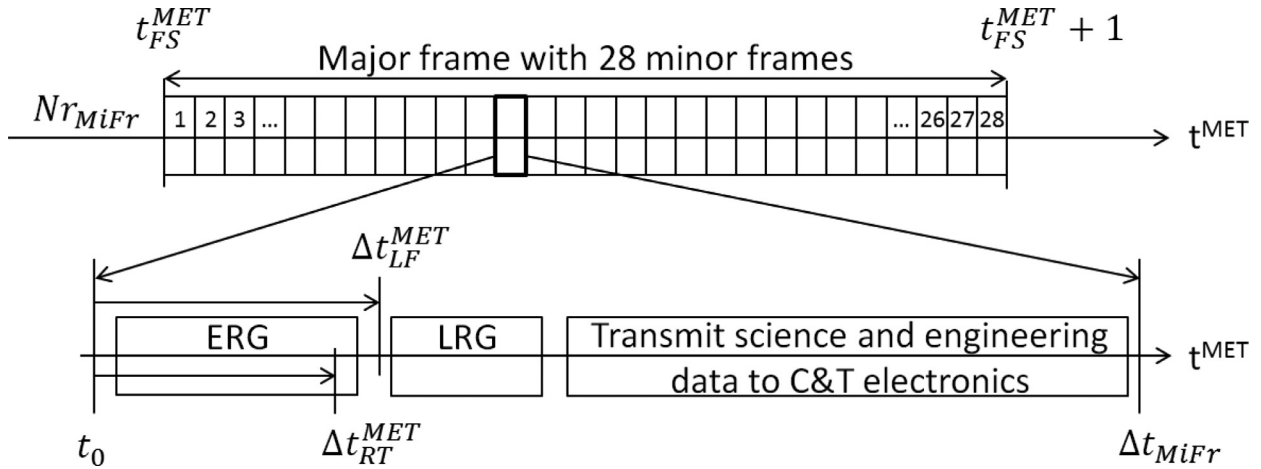


Fig. 2. Timing of a LOLA major frame with its 28 minor frames (N_{rMiFr}) which is spanning over one full second (t_{FS}^{MET}). All events are measured in Mission Elapsed Time (MET). One frame contains the Earth Range Gate (ERG) and the Lunar Range Gate (LRG). Both the laser receive time (Δt_{RT}^{MET}) and the LOLA laser fire time (Δt_{LF}^{MET}) are referenced to t_0 , which marks the beginning of a minor frame. The LOLA laser fires ≈ 9.6 ms after t_0 . The rest of the minor frame that has a total length of $\Delta t_{MiFr} \approx 35.7$ ms, is used to transmit science and engineering data to the Command & Telemetry (C&T) electronics.

at 14 Hz), the number of successful measurements is correspondingly smaller. For other stations ranging at 10 Hz (e.g. MOBLAS), shots fall on average at least twice per second in the Earth range gate (compare Table 1). A near-real-time feedback via radio with a delay down to 45 s helps the stations during operation to check whether shots are received and if they fire in phase with the LOLA cycle.

The timestamps for the detection of the incoming laser pulses are derived from the LRO onboard clock which is an Ultra Stable Oscillator (USO). While the ground station clocks have stabilities of 1×10^{-12} to 1×10^{-15} over periods of 10^3 to 10^7 s, the LRO onboard clock achieves its best stability of 7×10^{-14} after an averaging period of 40 s (see Table 2). Generally it is at 1×10^{-13} between 1 and 100 s and at 2×10^{-13} up to 10,000 s at constant temperatures (Cash et al., 2008). This stability adds up to an error in the range of 0.3 to 3 mm and up to 60 cm respectively. The accumulating range error becomes larger than the LOLA timestamp precision after 2500 s. Since the LRO USO stability does not become larger than 2×10^{-13} after an orbital period of LRO of ≈ 120 min (7200 s) no additional once per orbit error is introduced by the onboard clock.

Following Cash et al. (2008) the response of the LRO USO to temperature variation is $1\text{--}3 \times 10^{-12}$ / °C. We saw variations with an amplitude of 0.3 °C over one day which causes a maximum change in the rate of $0.3\text{--}0.9 \times 10^{-12}$ accordingly. Variations due to changes in the power consumption of close by instruments or the orbit height can cause further changes of the rate. These variations accumulate to an offset of 13–39 ns over one day, when we use a sinusoidal function for the integration of it. The resulting range error of $\approx 3\text{--}4$ m has an average linear trend of $1.5\text{--}4.5 \times 10^{-13}$. We observed remaining sinusoidal variations around the linear trend with amplitudes of $\approx 2\text{--}6$ ns. If we assume that a sinusoidal curve with a period of one day has a turnover point every 21,600 s, the remaining variations have an average rate of $\approx \pm 1\text{--}3 \times 10^{-13}$ between these points. Since the LRO clock stability is 2×10^{-13} over up to 10,000 s, this average rate is at or below this value. Since no correction was available for the change of the rate due to temperature change within our work yet, the resulting periodic and the further changes mix with the stochastic noise of the LRO clock. The incomplete corrections affect the approximation of it via the polynomial fits (see Sections 6.1, 6.2 and 7.2). Because the ground station clocks are not subject to temperature change due to proper housing, their approximation is only affected by their stability.

Compared to the LOLA timestamp precision of 15 cm, Exertier et al. (2006) reported random errors below that within Satellite Laser Ranging (SLR) in general. They found a 7 – 12 mm random error for Full Rate and 1 – 3 mm for Normal Point data. The errors are thereby coming from the ground station laser, detector, timer, clock and other dependencies as well as from the atmosphere and the target signature. Further the calibration of the station hardware, the atmosphere itself as well as the target signature introduce a systematic error of 8 – 19 mm. The systematic errors are larger than the random ones with the one-way setup as well. The errors are thereby coming from the LRO onboard and the ground station clocks, the orbit that we use for the predictions as well as the modeling accuracy of the environment (atmosphere) as it will be shown with the results (Section 7). The target signature error is not present with the one-way setup.

4. Time transfer via LRO laser ranging and other optical experiments

The two-way laser time transfer experiments T2L2 and ELT allow for the direct estimation of the offset between station and onboard clock (ground to space time transfer). This offset can be further used to measure the differences or synchronize remote ground station clocks (ground to ground time transfer). In case of T2L2 the offsets of all participating stations to the onboard clock are used to estimate the difference between them either in non-common and common view (Exertier et al., 2013).

Both the T2L2 and the ELT experiment feature a similar setup consisting of a retro-reflector, a detector (providing an active uplink) and a timing system and are tracked by ILRS ground stations. The T2L2 experiment was launched onboard the Jason2 satellite in 2008 and utilizes its USO (Exertier et al., 2013). The ELT experiment will make use of the Atomic Clock Ensemble in Space (ACES) onboard the International Space Station (ISS) which will include both an atomic clock and an H-Maser (Schreiber et al., 2009).

With the laser ranging to LRO we pair a predicted receive to a measured receive time to complete the one-way observable (Section 5.4). Unlike with the two-way T2L2 and ELT experiment an unbiased range measurement (via the retro-reflector) is not available in order to estimate the offset between the ground station and the onboard clock directly. Due to the prediction the ground to space time transfer is affected by orbit errors, modeling and random errors of the LRO clock and errors of the cor-

Table 3

Performance comparison of the T2L2, the ELT and the LRO laser ranging time transfer experiment taken from Exertier et al. (2006), Schlicht (2012) and the results of this work respectively. The performance is compared for ground to space and ground to ground time transfer in common view (CV) and non-common view (NCV).

Experiment	Setup	Ground to	Accuracy	Averaging period τ
T2L2	Two-way	Space	< 10 ps	1000 s
		Ground CV	\approx 10 ps	1000 s
		Ground NCV	150 ps	300 s
ELT	Two-way	Space	4 ps	300 s
		Ground CV	6 ps	300 s
		Ground NCV	7 ps	\approx 5400 s*
LRO LR	One-way	Space	166 ns**	56 days
		Ground CV	500 ps	\approx 2000 s***
		Ground NCV	–	–

* Dead time of one orbit cycle (Schlicht, 2012) which we assumed to \approx 90 minutes for the ISS.

** Accuracy estimated from the 1- σ variation of the post-fit measurement residuals (see the discussion in this section).

*** Average length of a LRO laser ranging pass (see Section 7.1).

rections (see Sections 6.2 and 7.2). However as it will be shown in Section 6.2 (multiple-pass analysis) and Section 6.3 (simultaneous pass analysis) we can estimate the differences between the ground station clocks. Thereby the multiplepass analysis allows for common and non-common and the simultaneous pass analysis for common view time transfer whereby the latter one is insensitive to orbit and LRO clock errors (see Section 6.3). The accuracy of the time transfer from the simultaneous passes is below LOLA's timestamp accuracy and thus only limited by the precision of the instrument which is 500 ps (see Section 6.3 and Sun et al., 2013b). Contrary the accuracy of the ground to space time transfer - which we measure from the 1- σ variation of the post-fit measurement residuals - is affected by the errors from the orbit, the LRO clock modeling, random errors and incomplete corrections.

Table 3 shows a comparison of the performance of the two-way T2L2 and the ELT as well as the one-way LRO laser ranging time transfer experiment. Both two-way experiments achieve accuracies around and below 10 ps for ground to space and ground to ground time transfer. With non-common view time transfer, the ELT achieves much better accuracies than the T2L2 experiment due to the more stable clocks (Atomic and H-Maser compared to USO - see Table 2) even over one ISS orbit. With that the ELT experiment will enable global time transfer between all stations that can range to its detector.

With the LRO laser ranging experiment we used polynomial fits for the characterization of the LRO clock from which we also derived the ground to space time transfer. Compared to the T2L2 and the ELT experiment the timeframes over which the ground to space time transfer is carried out are much longer (see Table 3). Comparing the accuracy (166 and 256 over 56 days and 5 years respectively) to the accuracy of the nominal LRO trajectory (30 ns), we see that the influence of the orbit errors is smaller than the other errors together. As it will be shown (see Sections 6.2, 6.3 and 7.3) ground to ground time transfer is only possible in common

view. Non-common view measurements would become subject of too much interpretation with the accumulated errors from the orbit, the modeling and the random errors of the LRO clock and the incomplete corrections. As reported by Sun et al. (2013b) and confirmed with our results in Section 7.3, the time transfer with common-view laser ranging observations to LRO achieves an accuracy of 500 ps over the average pass length.

Compared to the T2L2 experiment onboard the Earth-bound Jason-2 spacecraft, the distance between the ground stations and LRO is much larger. Due to the different observation geometry, the LRO laser ranging time transfer can tolerate larger uncertainties in the spacecraft positioning than the T2L2 project (Sun et al., 2013b). However since the T2L2 experiment was a dedicated time transfer experiment it still achieves a better performance than the time transfer carried out via the laser ranging to LRO (see Table 3).

5. Data processing methods

The laser measurements are affected by various influences that we correct for. While the corrections for atmospheric and relativistic effects cover systematic influences, the range walk correction addresses random errors that affect the data measurement precision. Following that the pairing of the separated one-way data and the formation of the Normal Point (NP) from the Full Rata (FR) data is described.

5.1. Correction for atmospheric effects

While the laser pulses travel through the atmosphere they are decelerated for which we apply an atmospheric correction Δt_{AC} to the measurements. Following Rothacher (2000) we can neglect the influence of the ionosphere on an optical signal. For the troposphere we use the standard model from Marini et al. (1973) where we input the environmental conditions recorded by the stations. The conditions, their change and the resulting correction are listed in Table 4 for an example pass where GO1L station ranged to LRO on September 14, 2009 at 15:52 UTC for \approx 45 minutes.

In contrast to ranging campaigns involving Earth satellites, the elevation change during a LRO pass and thus the change of the correction is small over a long timeframe (8° over 45 min - see Table 4). Also, the Lunar target is usually at high elevations, so that we set the correction to an averaged value, as shown in Table 4 with the example pass. While some stations provide continuous meteo measurements throughout their pass, many only provide one meteo measurement. Hence we use just one correction value for each passes. In case of the example pass this constant correction value causes an error in time of $\approx \pm 0.2$ m ($\approx \pm 0.7$ ns) and in rate of $\approx 5 \times 10^{-13}$ over the length of the pass (45 minutes). The error introduced by the simplified atmospheric correction is small than the other errors as it will be shown in Section 7.3.

The introduced rate difference of $\approx 5 \times 10^{-13}$ with the example pass (see Section 5.1) is only half the magnitude of the LRO clock random errors (2×10^{-13}) and the missing LRO clock rate correction due to temperature variation ($4.5 + 3 \times 10^{-13}$ at max) together ($\approx 1 \times 10^{-12}$). Furthermore the difference in rate is accumulating an

Table 4

Environmental conditions and resulting laser signal delay for an example laser ranging pass from GO1L station to LRO on September 14, 2009.

Time of the pass	Pressure in mbar	Temperature in K	Humidity in %	Elevation in °	Correction	
					in ns	in m
Begin	1010.0	299.65	68	53	10.3	3.09
End	1009.4	299.85	66	45	11.6	3.48
Difference	0.6	0.2	2	8	1.3	0.39
Averaged to					10.9	3.27

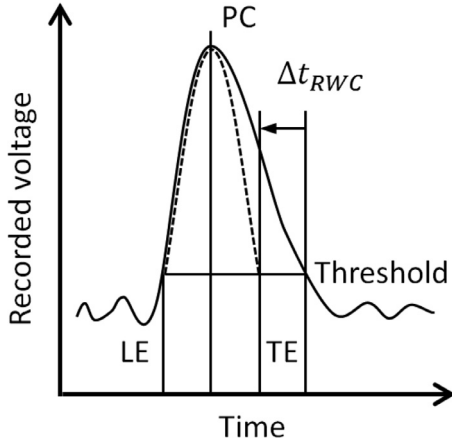


Fig. 3. The receive time of a recorded pulse is taken from the Peak Centroid (PC) which is averaged from the Leading Edge (LE) and Trailing Edge (TE) at a threshold. The range walk causes the trailing edge to be delayed which results in a biased receive time. The solid line represents the distorted and the dashed line the corrected pulse.

offset only throughout an individual pass if conditions are changing. Contrary the random LRO clock errors and errors due to the incomplete corrections are accumulating varying offsets over the whole clock arc length (e.g. 28, 56 days or 5 years).

Further atmospheric effects on laser ranging measurements such as attenuation, scintillation, and beam wander are below the LOLA measurement precision (Dirkx et al., 2014) and thus neglected within this analysis.

5.2. Correction for range walk

The LOLA time tags of the received pulses are affected by a range walk bias. Due to the impulse response of the LOLA detector electronics, the shape of a recorded receive pulse is distorted which causes the trailing edge to be delayed (see Fig. 3). Because the peak centroid is averaged from the leading and trailing edge at a threshold, the delay causes an offset on the receive times. Over a whole pass this correction reduces the measurement precision.

The single pulses are corrected for range walk with an empirical formula from Mao et al. (2011) via

$$\Delta t_{RWC} = 6.0 \cdot \sqrt{36.0 + P_{Station} \cdot (PW - 1)^2}, \quad (1)$$

where PW is the pulse width, measured in ns and $P_{Station}$ a station correction factor. We used a series of passes to estimate an optimal empirical correction factor for each station. First a correction factor was estimated for every pass following the requirement, that the measurement precision σ_{MP} becomes minimal. From that series of optimized values, a single $P_{Station}$ was averaged for every station as listed in Table 5. Due to a different pairing and processing our values are different to the values from Mao et al. (2011).

Without the range walk correction, the measurement precision is usually around 30 to 50 cm. After applying the correction the observation data reaches the LOLA timestamp precision of 15 cm. Even though the minimal measurement precision requirement is a simplified approach for the estimation of the station parameters, it is sufficient within the empirical formula.

5.3. Correction for relativistic effects

The rate of a clock is influenced by the gravitational potential ϕ at its location and its velocity v with respect to the solar system barycenter. Since a ground station and the LRO clock are at different locations and move with different velocities, we correct the

Table 5
Estimated $P_{Station}$ values for the various ground stations.

Code	ID	$P_{Station}$
MDOL	7080	0.18
YARL	7090	0.20
GODL	7105	0.19
MONL	7110	0.21
GO1L	7125	0.10
HARL	7501	0.20
ZIML	7810	0.19
HERL	7840	0.21
GRSM	7845	0.19
WETL	8834	0.21

measurements for the resulting differences due to relativistic effects. While the station fire times are converted from UTC to TDB with Eq. (8) from Section 5.4, we derive a relationship between TDB and MET for the LRO clock in the following. Further information on the transformation between various time scales can be found in Kaplan (2005).

The Barycentric Coordinate Time (TCB) represents the time measured by an atomic clock located at the Solar System Barycenter. Moyer et al. (1971) describe the influence on the rate of a clock by the gravitational potential ϕ at the clocks location and its velocity v with respect to the solar system barycenter with the ratio

$$\frac{dt^{Clock}}{dt^{TCB}} = \left[1 - \frac{2\phi}{c^2} - \left(\frac{v}{c} \right)^2 \right]^{\frac{1}{2}} \quad \text{by using } \phi = \sum \frac{\mu_i}{r_i} = \sum \frac{G \cdot m_i}{r_i}. \quad (2)$$

Thereby c is the speed of light and ϕ is calculated from the gravitational parameter μ_i of the planets and their distance r_i with respect to the spacecraft.

By using Eq. (2) the difference in rate between the LRO clock which measures MET and TCB is

$$\frac{dt^{MET}}{dt^{TCB}} = \left[1 - \frac{2\phi_{LRO}}{c^2} - \left(\frac{v_{LRO}}{c} \right)^2 \right]^{\frac{1}{2}}. \quad (3)$$

Thereby we calculate the potential at the location of the spacecraft with respect to the Solar System Barycenter with

$$\phi_{LRO}(t) = \sum \frac{\mu_i}{|r_{i-LRO}(t)|} = \frac{\mu_{SUN}}{|r_{SUN-LRO}(t)|} + \frac{\mu_{EARTH}}{|r_{EARTH-LRO}(t)|} + \frac{\mu_{MOON}}{|r_{MOON-LRO}(t)|}. \quad (4)$$

Following (Kaplan, 2005) TDB only differs constant in rate to TCB and is defined as

$$\frac{dt^{TDB}}{dt^{TCB}} = 1 - L_b = 1 - 1.550519768 \times 10^{-8}. \quad (5)$$

By combining Eq. (3) and (5) we can describe the difference in rate between MET and TDB with the ratio

$$\frac{dt^{MET}}{dt^{TCB}} / \frac{dt^{TDB}}{dt^{TCB}} = dt^{MET} / dt^{TDB} = \frac{\left[1 - \frac{2\phi_{LRO}}{c^2} - \left(\frac{v_{LRO}}{c} \right)^2 \right]^{\frac{1}{2}}}{1 - L_b}. \quad (6)$$

Fig. 4 shows the difference in rate plotted as $dt^{MET}/dt^{TDB} - 1$ between MET and TDB throughout the year 2010. The annual variation due to the elliptical orbit of the Earth-Moon system around the Solar System Barycenter and the 28 day variation due to the orbit of the Moon around the Earth can be identified. In addition, there is the variation due to the orbit of LRO around the Moon with a period of ≈ 120 minutes (see Fig. 5). By integrating the difference in rate over time from an epoch t_e we can derive the offset

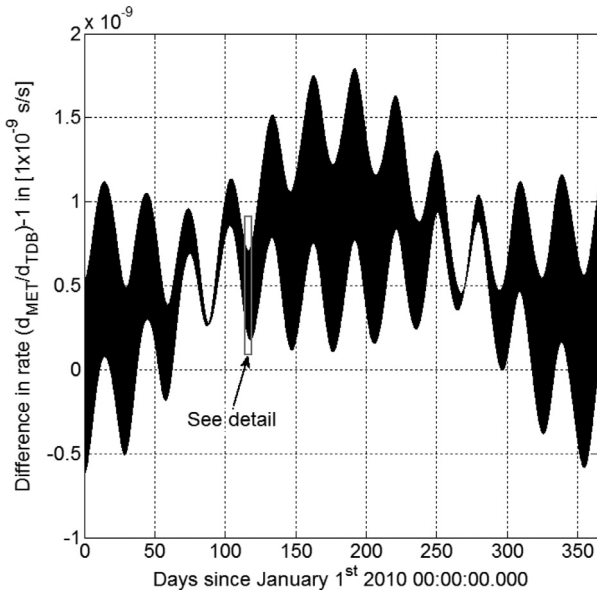


Fig. 4. Normalized difference in rate between MET and TDB throughout 2010. Variations due to the orbit of LRO around the Sun and the Earth are visible.

between MET and TDB for a certain date t_d with

$$\Delta t_{RC} = \int_{t_e}^{t_d} \frac{dt^{MET}}{dt^{TDB}} dt. \quad (7)$$

5.4. Pairing of the fire and receive times

As the fire and receive events are recorded separately at the ground stations and on board of LRO, the two independent clock readings have to be paired in order to establish the complete range measurement. Such pairs are also called biplets within the SLR community. In case of two-way experiments such as T2L2 that carry a detector and a retroreflector such pairs are called triplets (Exertier et al., 2011).

The fire times from the stations are converted by using

$$t^{TDB} = t^{UTC} + 32.184 + \Delta t_{LS} + \Delta t_{PT} \quad (8)$$

from Kaplan (2005), where t^{TDB} is the resulting TDB time from a given UTC time t^{UTC} . Δt_{LS} is the number of leap seconds for a given year and Δt_{PT} are the periodic terms which incorporate the eccentricity of the Earth orbit and perturbations of it by other planets. The derivation of the formula and the precise calculation of the Δt_{PT} can be found in Moyer et al. (1981).

We use the nominal LRO trajectory in form of the Spacecraft and Planet Kernel (SPK) within the software SPICE to get a predicted TDB receive time t_{PRT}^{TDB} from

$$t_{FT}^{TDB} + \Delta t_{LT}^{TDB} + \Delta t_{AC} = t_{PRT}^{TDB}. \quad (9)$$

t_{FT}^{TDB} is the TDB fire time at the ground station, Δt_{LT}^{TDB} the predicted light time from the nominal LRO trajectory and Δt_{AC} the correction for atmospheric effects (see Section 5.1). While the fire times from the station are influenced by the accuracy of the station calibration, the light time is affected by the nominal trajectory accuracy.

We calculate the MET receive time t_{RT}^{MET} from the single parts contained in the RDR files (see Fig. 2) to which we apply the corrections with

$$t_{RT}^{MET} = t_{FS}^{MET} + Nr_{MiFr} * \Delta t_{MiFr} + \Delta t_{RT}^{MET} + \Delta t_{RWC} + \Delta t_{RC}. \quad (10)$$

Thereby t_{FS}^{MET} are the full MET seconds, Nr_{MiFr} the number of the minor frame, Δt_{MiFr} the length of a minor frame and Δt_{RT}^{MET} the MET receive time of a pulse after t_0 . We correct for range walk

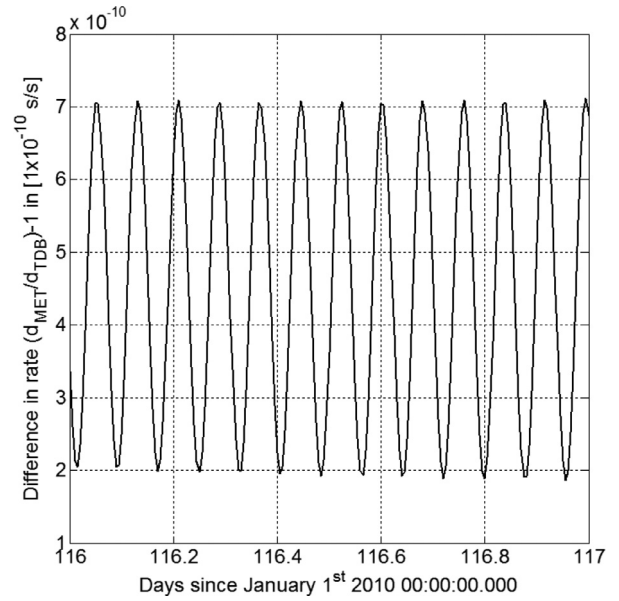


Fig. 5. Detail of the normalized difference in rate between MET and TDB for one day. Note the different scales. Variations due to the orbit of LRO around the moon are visible.

Δt_{RWC} and relativistic effects Δt_{RC} as described in Sections 5.2 and 5.3 respectively.

The RDR files also contain the LOLA laser fire event in MET and converted with the SCLK in UTC which we further convert to TDB with Eq. (8). We derive a TDB converted receive time t_{CRT}^{TDB} from a MET receive time t_{RT}^{MET} by using a linear fit applied to these LOLA laser fire events. The accuracy of the SCLK conversion is ± 3 ms coming from the accuracy of the SCLK (see Fig. 1). Even though this accuracy is too coarse for laser ranging data analysis itself, it is sufficient for the pairing. Since a single Earth Range Gate does not record more than one laser pulse and the cycle frequency is 28 Hz, the time between consecutive receiving events is always at least ≈ 0.0277 s. This setup enables the unique identification of a pair even at an accuracy of ± 3 ms.

We identify all converted receive times t_{CRT}^{TDB} as potential receives that range 0.1 s around a predicted receive time t_{PRT}^{TDB} for every fire time t_{FT}^{TDB} of a pass. By saying that the difference Δt_{RT}^{TDB} between the predicted and the converted receive times shall become minimal, we can find a corresponding pair with

$$\Delta t_{RT}^{TDB} = t_{PRT}^{TDB} - t_{CRT}^{TDB}. \quad (11)$$

By comparing Δt_{RT}^{TDB} for all paired shots of a pass, offsets can be detected and outliers removed in an iterative process. The derived TDB and MET link becomes more accurate after replacing the TDB converted receive times t_{CRT}^{TDB} with the predicted TDB receive times t_{PRT}^{TDB} from the nominal LRO trajectory.

Figs. 6 to 8 show the pairing of an observation pass from November 15, 2011 when the WETL station in Southern Germany was ranging to LRO between 00:51 and 01:24 UTC. Fig. 6 shows the light time of the predicted (Δt_{LT}^{TDB}) and the paired converted receiving events ($t_{PRT}^{TDB} - t_{CRT}^{TDB}$) which have a difference of 535.3 μ s on average throughout this pass. The difference shown in Fig. 7 is caused by the limited SCLK accuracy. By fitting a 4th order polynomial to this difference Δt_{RT}^{TDB} , we can remove the observed offsets and trends and yield the measurement precision σ_{MP} of the laser ranging pass from the 1- σ variation as shown in Fig. 8. For this particular pass we find a precision of 7.70 cm, which attests the high quality of the ranging experiment. Fig. 8 also shows the measurement precision of the NP data that is averaged from the FR data as described in the next section.

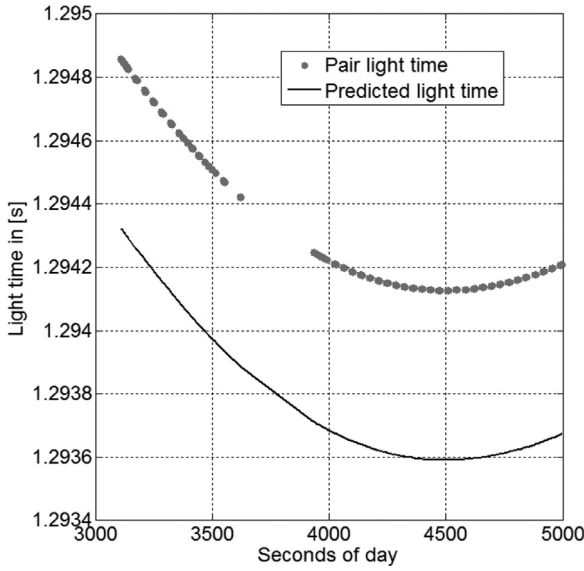


Fig. 6. Light time for the prediction from the nominal LRO trajectory (line) and the paired shots that were converted with the SCLK (dots).

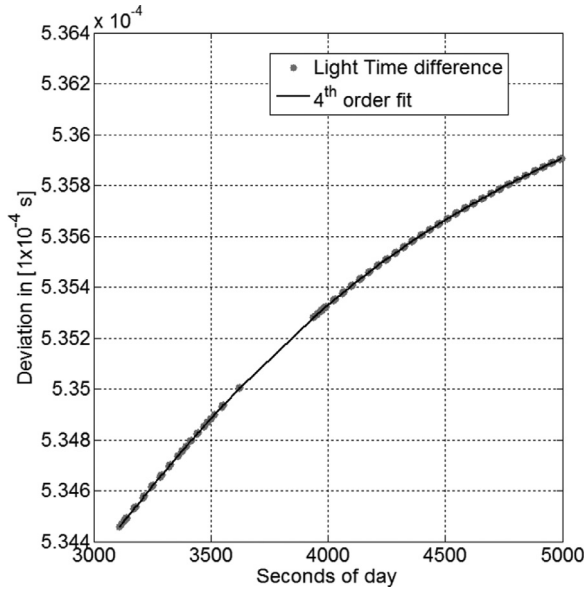


Fig. 7. Difference between the light time of the prediction and the paired shots (dots). 4th order fit (solid line) added.

5.5. Normal point formation

NP's are the official station data product for SLR observations within the ILRS community (Torrence et al., 1984). The formation from the FR data reduces the data amount, while improving precision and balancing station system dependent variations via an averaging. Because of these advantages we use NP's that have all corrections applied within the further applications.

Our NP's incorporate the TDB fire, the TDB predicted receive and the MET receive time. Following the NP formation guidelines of Torrence et al (1984), the observations are grouped into bins which start at midnight. As defined by the ILRS guideline for LRO, the bin length is 5 seconds and a NP is formed if there is more than 1 observation per bin (ILRS website, 2016). We use the TDB predicted receive times for the binning and group the MET receive times accordingly in order keep up the previously derived pairing.

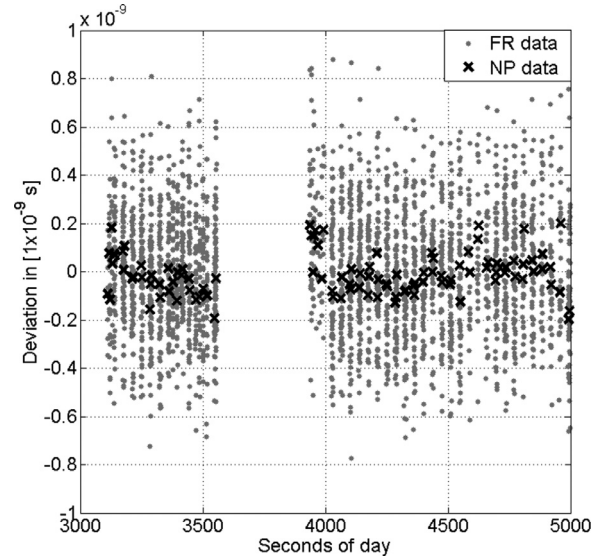


Fig. 8. Deviation of the paired shots with respect to the 4th order fit from which the measurement precision is derived. Deviation is shown in dots for the FR and in asterisks for the NP data.

In case of the example pass the measurement precision σ_{MP} reduces from 7.70 to 2.60 cm and the number of paired shots from 2791 to 104 after the averaging of the FR to the NP data (see Fig. 8). The reduction of the data volume simplifies the processing of a larger number of passes in further applications.

6. Data analysis methods

This section describes how we utilize single, multiple and simultaneous passes to derive the experiment and ground station performance, characterize the LRO clock and the ground station clock differences by time transfer. We model the LRO and the ground station clock differences with polynomial fits after applying the corrections to the measurements.

6.1. Single-pass analysis

We analyze the single passes of the dataset regarding the criteria described in the following and shown in Fig. 9. From the overall or per station averaged values we derive the statistical experiment and the station performance respectively. The measurement precision σ_{MP} is derived from the 1- σ variation of the receive times as described in Section 5.4.

From the number of fired shots $N_{r_{FS}}$ and the pass length Δt_{PL} we get the station fire frequency

$$f_{SF} = N_{r_{FS}} / \Delta t_{PL} . \quad (12)$$

With the number of paired shots $N_{r_{PS}}$ and the pass length Δt_{PL} we get the paired shots per second as a frequency via

$$f_{PS} = N_{r_{PS}} / \Delta t_{PL} . \quad (13)$$

We calculate the ratio between the number of fired and paired shots with

$$Rat_{ptFS} = N_{r_{PS}} / N_{r_{FS}} . \quad (14)$$

Further we characterize the LRO clock from the single-passes by applying a first order linear fit $f_{Single-pass}$ on the TDB and MET

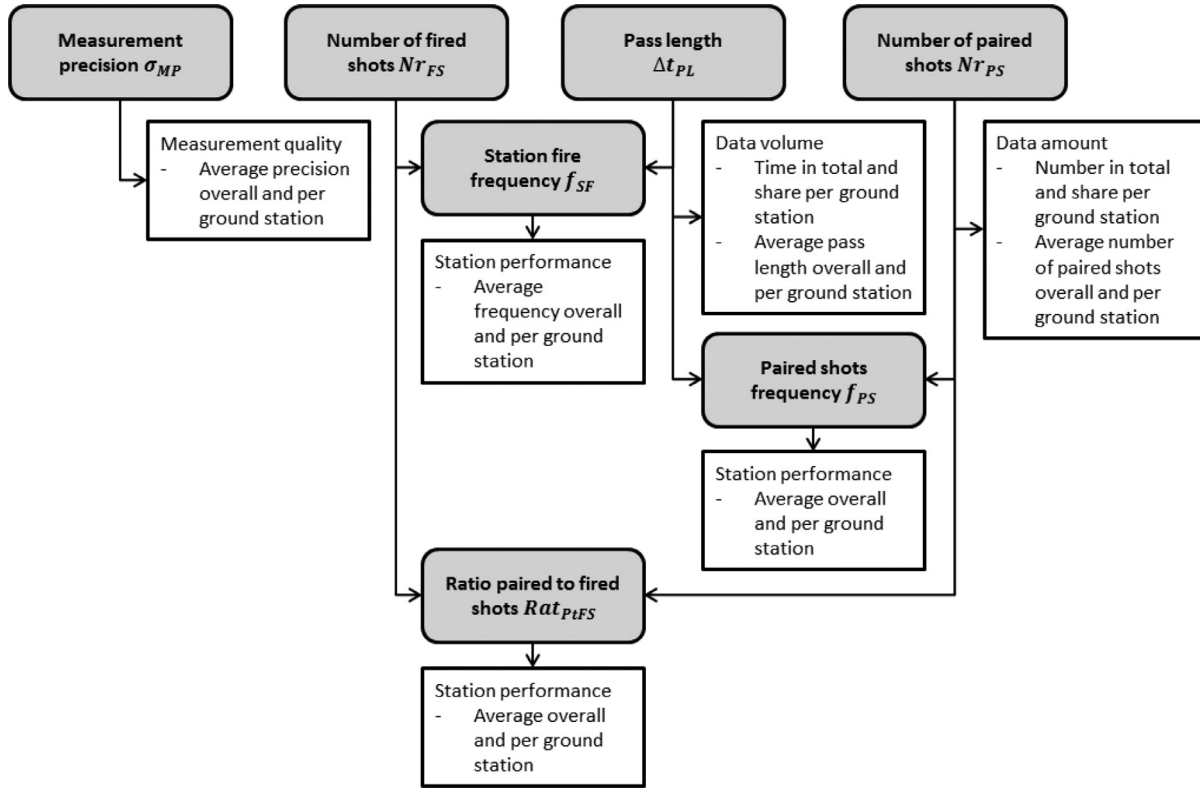


Fig. 9. Single pass analysis criteria and derived properties.

receiving times from which we measure the parameters offset $\Delta\tau_{Single-pass}^{(0)}$ and rate $\Delta\tau_{Single-pass}^{(1)}$ with

$$t^{MET} - t_0^{MET} = f_{Single-pass}(t^{TDB}) = \sum_{i=0}^1 \Delta\tau_{Single-pass}^{(i)} \times (t^{TDB} - t_0^{TDB})^i. \quad (15)$$

We use the paired measured MET and predicted TDB receive times for t^{MET} and t^{TDB} respectively with t_0^{MET} and t_0^{TDB} being their reference epoch respectively.

We do not estimate the higher order parameters clock parameters aging $\Delta\tau_{Single-pass}^{(2)}$ and its change $\Delta\tau_{Single-pass}^{(3)}$ from single passes since they are too short. While a single pass is ≈ 33 minutes long on average (see Section 7.1), the LRO clock aging value is around 1.6×10^{-12} /day² over all mission phases (see Section 7.2). This aging value causes an offset of 71 ps over the length of an average pass which is equivalent to 2.1 cm. Since this offset is below the LOLA time stamp precision the higher order parameters cannot be measured from the single passes directly but from the long term change of the rate.

The LRO clock parameters estimated from the single passes are affected by random errors of the LRO clock, the incomplete corrections as well as by errors from the nominal LRO trajectory. Systematics and trends on the predicted receive times from the nominal trajectory as well as on the predicted and the measured receive times from the random LRO clock errors and the incomplete corrections over a single pass introduce errors on the estimated LRO clock parameters.

6.2. Multiple-pass analysis

Beside the single-pass analysis, we use a 3rd order polynomial fit applied to multiple passes consecutive in time to approximate the actual LRO clock trend as shown in Fig. 10. We characterize the

LRO clock by estimating its parameters offset, rate, aging and its change from the fit and the ground station clock differences from the pass residuals with respect to it (ground to ground time transfer). Further the fit provides referencing of the MET to the TDB time scale (ground to space time transfer) similar to the SCLK (see Section 2 and Fig. 10).

The timeframe over which we apply the fit typically is one mission phases (≈ 28 days) since the nominal LRO trajectory is grouped accordingly. Changes of the LRO clock rate due to external effects can further shorten the timeframe. If the fit is applied over longer timeframes (e.g. multiple mission phases) the pass residuals will feature jumps due to the grouping of the nominal trajectory.

The 3rd order fit provides the offset $\Delta\tau_{Multi-pass}^{(0)}$, the rate $\Delta\tau_{Multi-pass}^{(1)}$, the aging $\Delta\tau_{Multi-pass}^{(2)}$ and its change $\Delta\tau_{Multi-pass}^{(3)}$ via

$$t^{MET} - t_0^{MET} = f_{Multi-pass}(t^{TDB}) = \sum_{i=0}^3 \Delta\tau_{Multi-pass}^{(i)} \times (t^{TDB} - t_0^{TDB})^i. \quad (16)$$

As within Eq. (15) we use the paired measured MET and predicted TDB receive times for t^{MET} and t^{TDB} respectively. A manual editing is used to remove outlying passes while applying the fit.

Furthermore we characterize the differences between the ground station clocks in time and rate from the pass residuals of common view observations with respect to the fit as shown in Fig. 11 (ground to ground time transfer). The relative offsets and rates between simultaneous passes (e.g. from GS1 and GS2 in Fig. 11) are derived from the difference between the estimated offsets with

$$\Delta\tau_{Multi-pass\ GS1\ GS2}^{(0)} = \Delta\tau_{GS1}^{(0)} - \Delta\tau_{GS2}^{(0)} \quad (17)$$

and the rates with

$$\Delta\tau_{Multi-pass\ GS1\ GS2}^{(1)} = \Delta\tau_{GS1}^{(1)} - \Delta\tau_{GS2}^{(1)}. \quad (18)$$

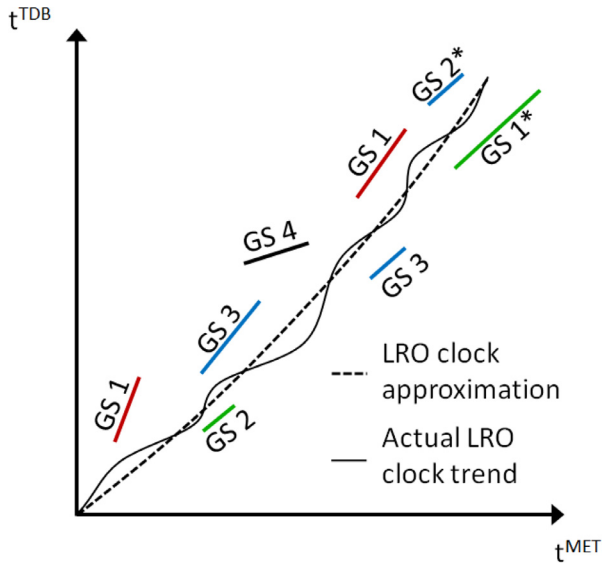


Fig. 10. Approximation of the actual LRO clock trend from multiple passes and their individual TDB and MET links, different ground stations (GS) are indicated by their labels, solid line represents the actual LRO clock trend and the dashed line the approximation from the 3rd order fit. The passes marked with an * are simultaneous passes (common-view observations). (For interpretation of the references to colour in this figure legend, the reader is referred to the web version of this article.)

Even though the fit features jumps if applied over more than one mission phase, it allows to monitor the long term station timing behavior with respect to each other.

The approximation from the 3rd order fit does not exactly represent the actual LRO clock trend (see Figs. 10 and 11). Deviations between the approximation and the actual LRO clock trend can be seen in the post-fit measurement residuals. Remaining trends and systematics in the residuals are caused by random LRO clock errors, incomplete corrections and the nominal LRO trajectory.

Pass residuals which we also use for the analysis of ground station clock differences during SM02 and SM03 in Section 7.3, are shown in Fig. 15. Table 6 provides an overview about the characteristics (accuracy from the $1-\sigma$ variation of the residuals, length as well as data coverage) of fits we applied during the mission phases SM02 and SM03 (see Sections 8 and 7.3). Since the reported accuracy of the nominal trajectory ($9\text{ m} \approx 30\text{ ns}$) is more than 5 times smaller than the accuracy of the fits, the random errors of the LRO clock and the errors from the incomplete corrections are larger.

To a certain extent random errors and missing corrections can be compensated by the polynomial fit. But the long-term approximation cannot cover all short-term variations due to the limited order of the fit. However due to the averaging of the fit the referencing of MET to TDB is possible even with data gaps of up to 3 and 5 days (see Table 6). Even though the approximation of the actual LRO clock trend is probably even less good during the data gaps compared to when observation data is available, the continuous coverage is provided.

Even though the long-term approximation does not represent the short term variations of the LRO clock very well, ground station clock differences can be measured from common view observations. The differences are thereby less affected from LRO clock approximation, orbit, random LRO clock and correction errors than the referencing itself. In an ideal case the errors would cancel out during a common-view observation (see Section 6.3 as well as Figs. 10 and 11). However some errors are present within the multiple-pass analysis and affect the measurements from common-view observations (see Section 7.3). The measurement of differences from consecutive passes (non-common view time transfer) becomes un-

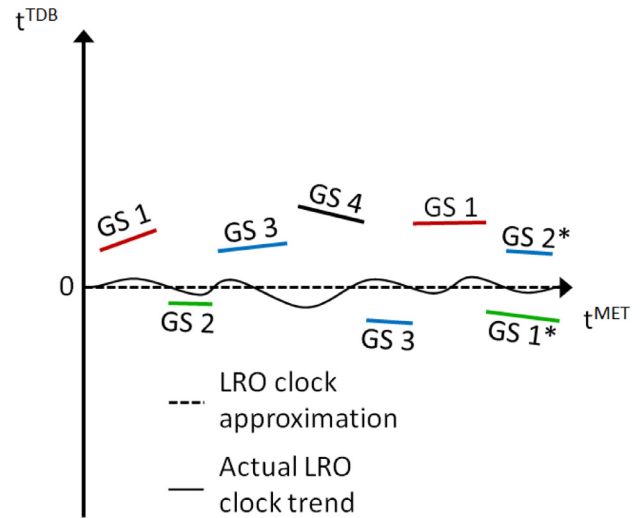


Fig. 11. Residuals of multiple passes with respect to the LRO clock approximation (dashed line), from which relative offsets and rates between the ground station passes can be derived. The actual LRO clock trend is added for comparison. The passes marked with an * are simultaneous passes (common-view observations). (For interpretation of the references to colour in this figure legend, the reader is referred to the web version of this article.)

Table 6

Laser data coverage and pass residuals with respect to the 3rd order polynomial fits that were applied during the mission phases SM02 and SM03.

Mission phase	SM02	SM03
Length in days	28	26
Number of selected passes	66	88
Average gap between consecutive passes in hours	9.16	5.94
Largest gap between consecutive passes in days	≈ 5	≈ 3
Pass residuals with respect to the fit from their $1-\sigma$ variation in ns	170.97	160.08

feasible since too many errors are accumulating between passes. Furthermore the nominal LRO trajectory error (30 ns) was at the order of magnitude of the ground station clock differences in some cases (see Section 7.3), limiting the validity of the measured values.

6.3. Simultaneous passes

While usually one station is scheduled to range to LRO at a time, also simultaneous ranging by multiple stations is possible, as long as all stations are in the field of view of the receiver. These common-view observations allow the measurement of timing differences (time transfer) of the participating ground station clocks. The measured differences are thereby insensitive to orbit and LRO clock errors and are resolved at the LOLA time stamp precision of 500 ps (Sun et al., 2013b).

In total we saw approximately 1215 simultaneous sessions within our dataset consisting of two or more stations ranging to LRO. For $\approx 52\%$ of them the time in between consecutive simultaneous passes was less than 0.5 days (≈ 5 LRO orbits). For 26% the time in between them was 0.5 to 1.5 days and for the other 21% 1.5 to 25 days. Almost all of the simultaneous passes were carried out between US stations. Because of the limited field of view of the Laser Ranging Telescope and the required pointing of the high gain communication antenna towards White Sands ground station simultaneous passes between US, EU and even Australian stations are mostly unfeasible.

Fig. 12 shows a simultaneous pass from the ground stations 7125 (GO1L) and 7110 (MONL) on November 29th, 2010 at 14:28

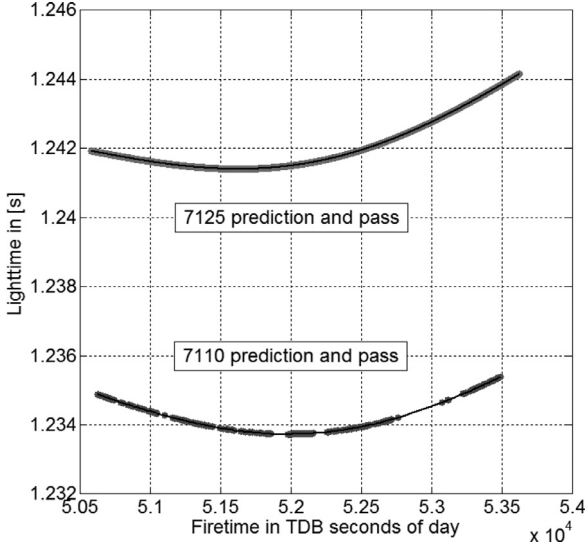


Fig. 12. Predicted and paired light times for the passes from 7125 and 7110 ground station. The paired receive times for the two ground stations are both represented with the same dots to highlight the fact that the LOLA detector cannot distinguish between the station pulses.

UTC. LOLA itself cannot distinguish the laser pulses coming from different stations and the first pulse in the Earth range gate closes it. We pair the fire and the receive times as described in Section 5.4 and apply all corrections. We use 4th order polynomial fits (f_{GS1} and f_{GS2}) on the paired predicted TDB and measured MET receive times of the passes from both stations. These fits provide links between MET and TDB for both ground stations with

$$t_{PRT\ GS1}^{TDB} = f_{GS1}(t_{RT}^{MET}) \text{ and } t_{PRT\ GS2}^{TDB} = f_{GS2}(t_{RT}^{MET}). \quad (19)$$

Here and in the following all TDB and MET times from the passes are normalized with t_0^{TDB} and t_0^{MET} derived from the pass starting first as in Eqs. (15) and (16).

Both fits (f_{GS1} and f_{GS2}) contain the signatures of the LRO clock as well as the respective ground station clock errors. Since the stations ranged to LRO simultaneously the difference between the LRO clock signatures contained within both fits is negligible. This fact implies that the variation of the LRO clock rate due to temperature change has no effect when measuring ground station clock differences from simultaneous passes. We thus measure the difference between the ground station clocks from the remaining differences after we corrected for the local atmospheric influence at the stations. Since incoming pulses cannot be detected concurrently by LOLA we derive the difference between the TDB times referenced to the same MET times from the fits via

$$\begin{aligned} & f_{GS1}(t^{MET}) - f_{GS2}(t^{MET}) \\ &= t_{RRT\ GS1}^{TDB} + \Delta t_{RRT\ GS1}^{TDB} - t_{RRT\ GS2}^{TDB} - \Delta t_{RRT\ GS2}^{TDB} \\ &= t_{RFT\ GS1}^{TDB} + \Delta t_{RFT\ GS1}^{TDB} + \Delta t_{LT\ GS1}^{TDB}(t_{RFT\ GS1}^{TDB} + \Delta t_{RFT\ GS1}^{TDB}) \\ & \quad - t_{RFT\ GS2}^{TDB} - \Delta t_{RFT\ GS2}^{TDB} - \Delta t_{LT\ GS2}^{TDB}(t_{RFT\ GS2}^{TDB} + \Delta t_{RFT\ GS2}^{TDB}). \end{aligned} \quad (20)$$

The TDB fire times t_{FT}^{TDB} from the stations are affected by clock offsets and we separate them into a real TDB fire time and an offset due to the station clock offset ($t_{RFT}^{TDB} + \Delta t_{RFT}^{TDB}$). Analogously we separate the predicted receive time t_{PRT}^{TDB} into a real TDB receive time and an offset propagated from the ground station clock offset ($t_{RRT}^{TDB} + \Delta t_{RRT}^{TDB}$).

The predicted TDB light time ($\Delta t_{LT}^{TDB}(t_{RFT}^{TDB} + \Delta t_{RFT}^{TDB})$) that we get from the nominal LRO trajectory is affected by the station offsets as well. Assuming a typical ground station offset of 100 ns and an orbital LRO velocity of ≈ 1 km/s we see that the spacecraft is

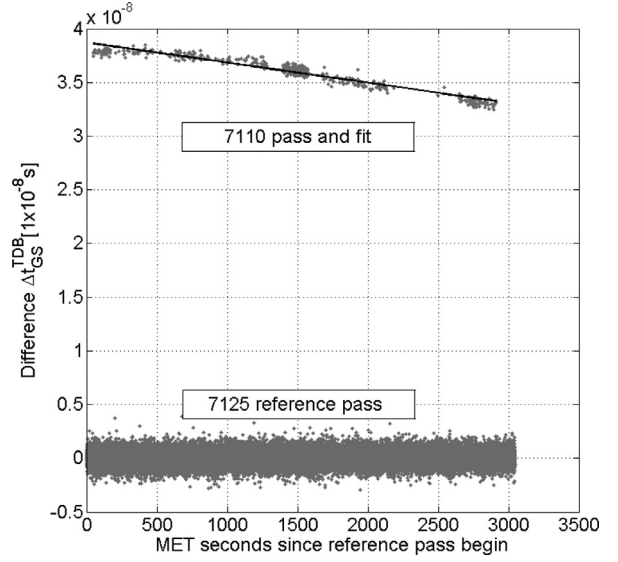


Fig. 13. Difference Δt_{GS}^{TDB} of the predicted TDB receive times paired to the same MET receive times from the two ground stations. The 7125 (G01L) pass is chosen as reference for the normalization since it is the pass starting first. A linear fit was applied to the 7110 pass to measure the timing differences.

moving 0.1 mm during such a time interval. Since this distance is equivalent to a difference of ≈ 0.3 ps in the light time, the influence of the ground station clock offsets on the predicted light time is negligible.

We regroup Eq. (20) for the difference of the ground station clocks, derive the predicted TDB light time $\Delta t_{LT\ GS1}^{TDB}(t_{RFT\ GS1}^{TDB})$ only from the real TDB fire time and get

$$\begin{aligned} & \Delta t_{RFT\ GS1}^{TDB} - \Delta t_{RFT\ GS2}^{TDB} \\ &= -t_{RFT\ GS1}^{TDB} - \Delta t_{LT\ GS1}^{TDB}(t_{RFT\ GS1}^{TDB}) + t_{RRT\ GS1}^{TDB} + \Delta t_{RRT\ GS1}^{TDB} \\ & \quad + t_{RFT\ GS2}^{TDB} + \Delta t_{LT\ GS2}^{TDB}(t_{RFT\ GS2}^{TDB}) - t_{RRT\ GS2}^{TDB} - \Delta t_{RRT\ GS2}^{TDB}. \end{aligned} \quad (21)$$

The difference of the real TDB fire time (t_{RFT}^{TDB}) plus the real predicted TDB light time ($\Delta t_{LT}^{TDB}(t_{RFT}^{TDB})$) to the real TDB receive time (t_{RRT}^{TDB}) is zero for both stations. Further the difference between the real predicted TDB receive times ($t_{RRT\ GS1}^{TDB} - t_{RRT\ GS2}^{TDB}$) in Eq. (20) is zero since perfectly synchronized clocks would provide identical MET to TDB links. With that we can simplify Eq. (21) to

$$\begin{aligned} & f_{GS1}(t^{MET}) - f_{GS2}(t^{MET}) \\ &= \Delta t_{RRT\ GS1}^{TDB} - \Delta t_{RRT\ GS2}^{TDB} = \Delta t_{RFT\ GS1}^{TDB} - \Delta t_{RFT\ GS2}^{TDB}. \end{aligned} \quad (22)$$

Thus the real ground station clock differences are equivalent to the modelled differences between predicted TDB receive times that are referenced to the same MET receive times via the fits (when assuming perfect ground station clocks in the model). We thus derive the ground station clock difference from the difference between the fits f_{GS1} and f_{GS2} for the same MET times. By applying a linear fit to the difference $f_{GS1}(t^{MET}) - f_{GS2}(t^{MET})$ throughout a simultaneous pass, we measure the relative offset $\Delta \tau_{Simu-pass\ GS1\ GS2}^{(0)}$ and the relative rate $\Delta \tau_{Simu-pass\ GS1\ GS2}^{(1)}$ between the ground station clocks GS1 and GS2 with

$$\Delta t_{GS}^{TDB} = \Delta t_{RRT\ GS1}^{TDB} - \Delta t_{RRT\ GS2}^{TDB} = \sum_{i=0}^1 \Delta \tau_{Simu-pass\ GS1\ GS2}^{(i)} \times (t^{MET})^i. \quad (23)$$

Since we work in the TDB time scale, we measure the ground station clock differences in TDB.

Fig. 13 shows the difference Δt_{GS}^{TDB} for the example, whereby the 7125 (G01L) pass provides the reference t_0^{TDB} and t_0^{MET} for the

Table 7

Laser ranging to LRO experiment and ground station performance derived from the overall and per station averaged values. The values are provided for the FR and the NPT data, if available. Various quantities are compared with their ratios.

ID Station Criteria	Type of data	7080 MDOL	7090* YARL	7105* GODL	7110* MONL	7125 GO1L	7501* HARL	7810 ZIML	7840 HERL	7845 GRSM	8834 WETL	Total or Average	Ratio
Station fire frequency in Hz	FR	8.74	9.95	9.12	9.49	26.81	9.52	11.34	13.06	7.93	10.77	11.68	4.36
Paired shots frequency in Hz	FR	0.76	1.10	0.93	1.25	13.14	0.74	2.98	3.98	0.86	1.09	2.68	
Ratio of paired to fired shots in %	FR	8.6	11.4	10.1	13.1	48.8	7.8	26.4	30.3	11.0	11.0	17.8	
Total pass length w.r.t. total amount of observation data in %	FR NP	10.33 10.10	20.30 19.89	6.49 6.12	24.70 24.64	32.96 34.23	0.90 0.83	1.52 1.50	0.47 0.48	2.06 1.92	0.27 0.27	3120.44 hrs 2918.13 hrs	1.07
Average pass length in seconds	FR	1846	1776	2651	2557	2431	1831	1294	1637	1566	2041	1963	–
Measurement precision in cm	FR NP	9.5 ± 3.1 5.5 ± 3.1	9.1 ± 1.9 3.8 ± 1.7	11.6 ± 4.5 7.4 ± 5.3	11.3 ± 4.8 7.5 ± 5.6	18.3 ± 4.1 8.3 ± 5.3	8.6 ± 2.3 4.0 ± 1.4	7.8 ± 0.8 2.2 ± 0.8	27.4 ± 10.6 7.8 ± 3.8	9.7 ± 4.8 3.9 ± 1.6	9.9 ± 7.7 5.7 ± 10.4	12.3 ± 4.5 5.6 ± 3.9	2.20
Nr. of paired shots w.r.t. total Nr. of shots in %	FR NP	1.49 6.70	4.40 18.97	1.21 5.05	5.89 25.4	85.11 39.88	0.13 0.53	1.03 1.34	0.35 0.57	0.33 1.46	0.06 0.11	64,865,805 1,558,657	41.61
Average Nr. of paired shots per pass	FR NP	1538 179	2223 241	2850 301	3522 378	36,248 418	1506 164	5064 167	7117 275	1438 168	2764 117	6427 241	26.67

* MOBILAS station

normalization since it is the pass starting first within the example common view observation. We measured a relative offset of ≈ 39 ns at the beginning of the pass and a relative rate of $\approx -1.9 \times 10^{-12}$ between the 7125 and the 7110 station clock.

7. Results

Section 7.1 provides the results of the statistical single-pass analysis from which we derive the experiment and the ground station performance. In Section 7.2 we present and compare the results of the LRO clock characterization coming from the single- and the multiple-pass analysis. Section 7.3 presents and compares the results of the ground station clock differences, estimated from the multiple-pass and the simultaneous pass analysis. We discuss the results and draw conclusions in Section 8.

7.1. Experiment and ground station performance

The laser ranging data covers a period from June 2009 until end of September 2014, including the mission phases Commissioning (CO), Nominal Mission (NO01 – NO13), Science Mission (SM01 – SM26) and Extended Mission (ES01 – ES25). The nominal LRO trajectory coverage begins July 13, 2009, while we started to process laser ranging passes from July 16, 2009 on. Due to missing orientation data the nominal LRO trajectory has gaps in coverage during mission phase ES25 (Mazarico, personal communication). Thus our dataset covers the timeframe from June 16, 2009 until the September 10, 2014 - the end of the mission phase ES24.

Table 7 shows the statistical results for all successfully paired and analyzed passes. While the stations fired at an overall average frequency of 11.68 Hz, 2.68 shots per second could actually be paired. In comparison to the predicted number of received shots per second (see Table 1), the number of actually paired shots per second is lower for all stations. While for most stations $\approx 10\%$ of the fired shots can be paired, GO1L achieves a ratio Rat_{PFS} of $\approx 49\%$ due to the synchronized firing to LOLA in frequency and phase. While the number of paired shots (6427 per pass on average) is heavily varying from station to station, the NP formation reduces (241 per pass on average) and balances the number of paired

shots between the stations. The average pass length Δt_{PL} is ≈ 33 minutes.

Altogether we successfully paired a total number of 64.9 million FR observations which got averaged to 1.6 million NP observations - a reduction by a factor of ≈ 41.7 . With the averaging of the paired FR shots to one NP every five seconds for every station, their paired shot shares become more balanced regardless their fire frequency.

We retrieved a total volume of 3120.44 hours of FR and 2918.13 hours of NP data. The NP data volume is smaller than the FR data volume, because NP's were only formed when there was more than 1 observation per bin (see Section 5.5). Further we only processed and analyzed passes that had more than 50 shots in case of the FR and more than 20 shots in case of the NP data. The largest share of tracking data in time comes from stations located in the US with $\approx 74\%$, while YARL station in Australia provides $\approx 20\%$ and the EU stations $\approx 5\%$.

The overall average measurement precision σ_{MP} of 12.3 cm confirms and even supersedes the LOLA time stamp accuracy of 15 cm and demonstrates the good precision of the one-way laser ranging data. With the NP formation the precision gets improved by a factor of 2.2 to 5.6 cm. The MOBILAS stations show similar performance with f_{SF} , Rat_{PFS} and σ_{MP} due to their similar equipment.

The shares of data volume we derived per station agree with values reported by McGarry et al. (2013) and Mao et al. (2014a) – see Table 8. We derived a different total volume than McGarry et al. (2013) since they analyzed the data early on during the experiment. Further our volume is different to Mao et al. (2014a) because of a different processing.

7.2. LRO clock analysis

We characterized the LRO clock by estimating its offset $\Delta\tau^{(0)}$, rate $\Delta\tau^{(1)}$, aging $\Delta\tau^{(2)}$ and its change $\Delta\tau^{(3)}$ on a single- and a multiple-pass basis as described in Sections 6.1 and 6.2 with data from the mission phases CO until ES24.

To compare the estimated parameters from both approaches the results from the single pass analysis were grouped and averaged mission phase wise as the fits were applied within the multiple-pass analysis. In order to derive the higher order parameters aging

Table 8
Laser ranging data volumes reported from different Authors.

Values from	MDOL	YARL	GODL	MONL	GO1L	HARL	ZIML	HERL	GRSM	WETL	Total in hours
This work	10.10	19.89	6.12	24.64	34.23	0.83	1.50	0.48	1.92	0.27	2918.13
McGarry et al. (2013)	11	15	9	28	33	1	1	1	1	<1	3489
Mao et al. (2014a)	10.91	14.31	7.78	28.58	32.71	0.76	1.48	1.46	1.90	0.12	4173.60

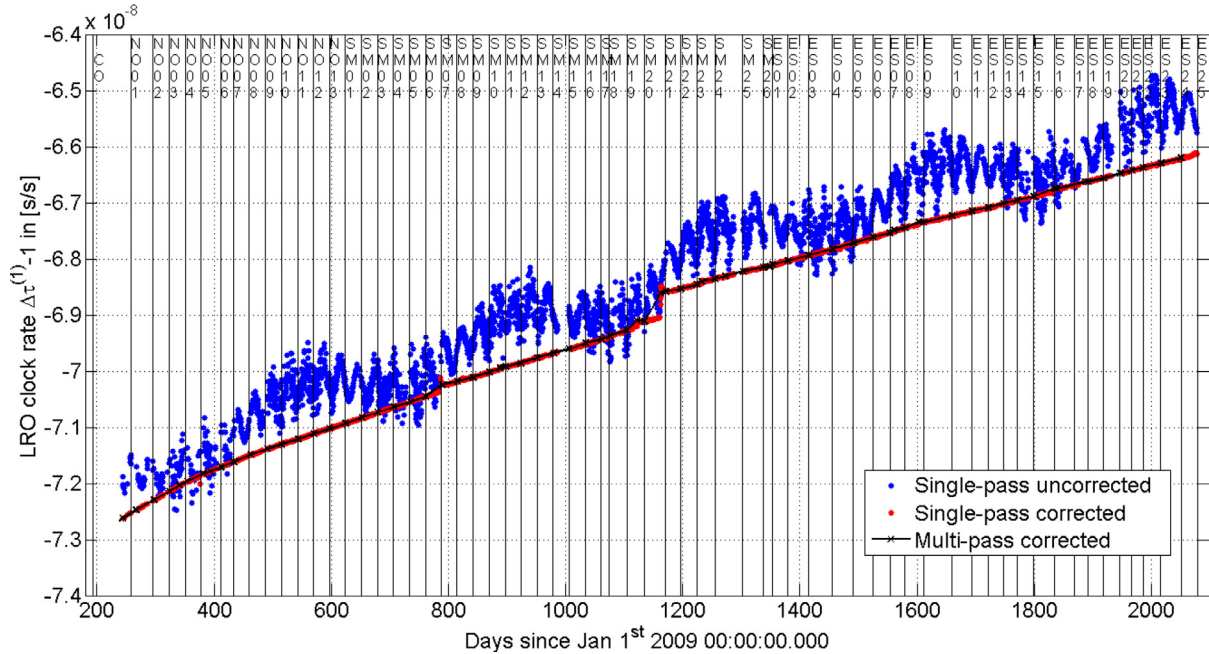


Fig. 14. Estimated LRO clock rate $\Delta\tau^{(1)} - 1$ on a single-pass basis uncorrected (blue dots) and corrected for relativistic effects (red dots). The LRO clock rate estimated from the multiple-pass analysis is represented by the black line with crosses for the data points. The various mission phases are marked by the vertical lines along with their names. (For interpretation of the references to colour in this figure legend, the reader is referred to the web version of this article.)

and its change from the single pass analysis, a 2nd order polynomial fit was applied to the estimated rates. Within some mission phases external events like solar flares influenced the clock and we further split the timeframe during one mission phase over which we apply the multiple-pass analysis fits. The single-pass analysis results were then grouped accordingly. Due to the grouping of the single-pass LRO clock parameters analog to the multiple-pass analysis for the comparison, the same averaging is applied. Due to that averaging, errors that affect the single-pass clock parameters (see Section 6.1) are compensated as within the multiple-pass analysis (see Section 6.2). Since both approaches are subject to the same random LRO clock errors, imperfect corrections and errors from the nominal trajectory, differences in the results are coming from the order of the applied fits and the averaging.

Since the ground station clocks have time biases with respect to each other, their single passes have varying time biases with respect to the mean trend of the multiple-pass analysis fit. We thus only evaluated the offset values $\Delta\tau^{(0)}$ from the multiple-pass analysis. Since they are represented in seconds at orders of 10 billion s and at LOLA timestamp precision (e.g. 35,049,494.9986398742 s at the beginning of ES09 and normalized to January 1, 2009 00:00:00.000) we focus on the presentation of the estimated rate, the aging and its change.

The estimated rate is shown and listed normalized via $\Delta\tau^{(1)} - 1$ in all figures and tables. Fig. 14 shows the LRO clock rate $\Delta\tau^{(1)} - 1$ estimated from both approaches, as well as the effect of the relativistic corrections. Variations with an annual monthly and orbital period (120 minutes) were detected in the LRO clock rate due to relativistic effects. The corrected clock rates from the single-

and multiple-pass analysis follow the same trend and show identical behavior regarding changes and jumps. Table SM.1 and SM.2 (Supplementary Material) provide the clock parameters rate, aging and its change estimated from both approaches and their differences for all mission phases (CO until ES24). Averaged clock parameters and their differences are given in Table 9.

The overall mean LRO clock rate is ≈ 8500 times larger than the $1-\sigma$ variation of the differences between the two approaches. Because of large changes in the LRO clock rate due to external influences during SM19 and SM20 (see Fig. 14), the differences of the parameters are larger than during other mission phases.

The overall mean aging value is ≈ 1.4 times larger than the $1-\sigma$ variation of the differences. For the change of the aging the overall mean value is ≈ 3.9 times smaller than the $1-\sigma$ variation of the differences (see Table 9).

The higher order terms aging $\Delta\tau^{(2)}$ and its change $\Delta\tau^{(3)}$ describe smaller changes than the rate (see Section 6.1) and are thus more sensitive to uncertainties. Since the nominal LRO trajectory is an averaged result from an orbit determination, the estimated parameters are affected by the inherent state errors. The precision of the estimated parameters is limited by the accuracy of the trajectory, the corrections and random LRO clock errors. The accuracy of the aging and the change of the aging depend on the length of timeframe over which they are averaged – e.g. one pass or one mission phase.

Our LRO clock rate agrees with the rate of Mao et al. (2014a) except for a small offset due to the selected reference. While we estimate our parameters with respect to TDB, Mao et al. (2014a) estimated them with respect to the GO1L clock.

Table 9

LRO clock parameters estimated from single- and multiple-pass analysis and their differences. The results from Table SM.1 and SM.2 were averaged over the mission phases as listed.

Averaged Mission phase	Day since Jan 1st 2009	Single-pass analysis			Multiple-pass analysis			1- σ variation of the differences		
		$\Delta\tau^{(1)}$ -1 10^{-8}	$\Delta\tau^{(2)}$ 10^{-12} /day	$\Delta\tau^{(3)}$ 10^{-14} /day ²	$\Delta\tau^{(1)}$ -1 10^{-8}	$\Delta\tau^{(2)}$ 10^{-12} /day	$\Delta\tau^{(3)}$ 10^{-14} /day ²	$\Delta\tau^{(1)}$ 10^{-12}	$\Delta\tau^{(2)}$ 10^{-12} /day	$\Delta\tau^{(3)}$ 10^{-14} /day ²
CO	250.87	-7.2627	4.41	-2.99	-7.2624	3.77	-0.13	-2.93	0.65	-2.87
NO01 – NO13	435.85	-7.1692	2.08	0.63	-7.1692	2.26	-1.12	6.85	0.49	2.13
SM01 – SM26	1014.92	-6.9468	1.58	-5.06	-6.9469	2.07	-8.61	10.55	1.59	10.99
ES01 – ES24	1725.63	-6.7103	1.11	-1.05	-6.7103	0.99	-1.96	5.22	0.76	9.07
CO – ES24	1144.77	-6.9103	1.54	-1.69	-6.9104	1.75	-2.99	8.11	1.18	9.20
Averaged from both approaches during CO-ES24: rate, aging, change of aging								-69,103.5	1.64	-2.34

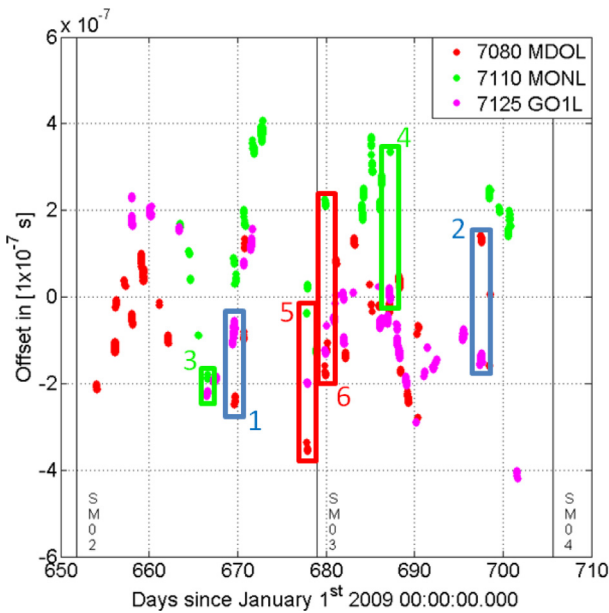


Fig. 15. Relative ground station offsets $\Delta\tau_{Multi-pass\ GS1\ GS2}^{(0)}$ measured from the time residuals with respect to the averaged trend from the multiple-pass analysis. The boxes highlight the data from two ground stations which were used to estimate the relative offset. The measured values can be found via their numbers in Table 10. (For interpretation of the references to colour in this figure legend, the reader is referred to the web version of this article.)

The fit from the multiple-pass analysis provides a referencing of the TDB and the MET time scale similar to the SCLK-based conversion (ground to space time transfer). We estimate the accuracy of this referencing from the 1- σ variation of the pass residuals with respect to the averaged trend (see Fig. 11, Table 6 and Fig. 15). The 1- σ variation of the pass residuals over both mission phases SM02 and SM03 is 166.25 ns. This value supersedes the accuracy of the SCLK based conversion by a factor of $\approx 18,000$. When analyzing the residuals throughout all processed mission phases (CO – ES24), we achieved a 1- σ variation of 256.07 ns, which is $\approx 11,700$ times better than the accuracy of the SCLK based conversion. For this result many GO1L passes were manually edited along with other outliers due to offsets at the 10 μ s magnitude with respect to the other ground station clocks. Since the accuracy of the nominal LRO trajectory is reported to be 30 ns (9 m at the arc overlaps) its influence on the accuracy of the referencing is smaller than the random LRO clock errors and the errors from the incomplete corrections.

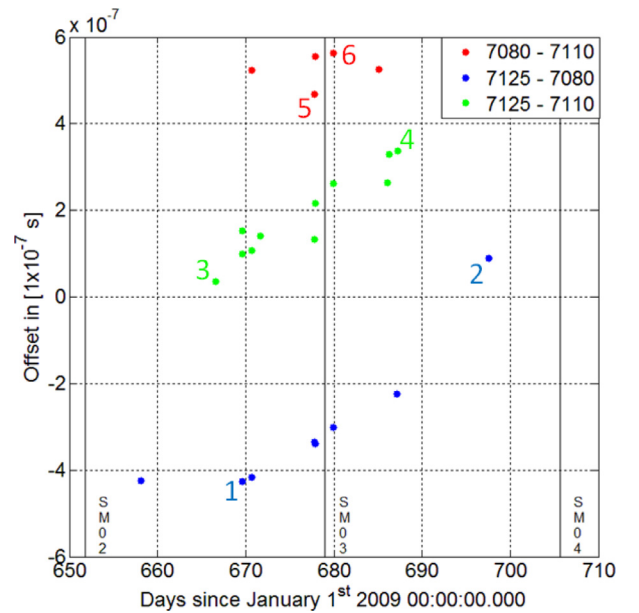


Fig. 16. Relative ground station offsets $\Delta\tau_{Simu-pass\ GS1\ GS2}^{(0)}$ measured from the simultaneous passes. The measured values can be found via their numbers in Table 10. All relative offsets measured from the simultaneous passes increase over time. (For interpretation of the references to colour in this figure legend, the reader is referred to the web version of this article.)

These errors are compensated by the averaging of the 3rd order fit to some extent. The accuracy of the estimated LRO clock parameters and the TDB and MET link (ground to space time transfer) demonstrate the potential of the laser ranging data for these applications.

7.3. Ground station clock analysis from time transfer

We used both the multiple-pass analysis and the simultaneous pass analysis to derive the timing differences between ground station clocks. We measured the relative offsets $\Delta\tau_{GS1\ GS2}^{(0)}$ and rates $\Delta\tau_{GS1\ GS2}^{(1)}$ with both approaches and compare their results.

We chose the mission phases SM02 and SM03 for a comparison, because we found good coverage with simultaneous passes between the three stations 7080 MDOL, 7110 MONL and 7125 GO1L. We focused on these three US stations due to limited coverage of simultaneous passes with other stations. During that timeframe we successfully paired eleven passes between two and five passes be-

Table 10

Comparison of relative ground station (GS) clock offsets $\Delta\tau_{GS1\ GS2}^{(0)}$ measured from the multiple-pass and the simultaneous pass analysis.

Station combination		Days since Jan 1st 2009	Nr.	Relative GS offset in ns measured from		Ratio
GS 1	GS 2			Multiple-pass analysis	Simultaneous pass	
GO1L	MDOL	669.7	1	−190	−430	+2.26
7125	7080	697.5	2	+280	+90	+3.11
GO1L	MONL	666.6	3	+33	+35	+1.06
7125	7110	687.2	4	+340	+340	+1.00
MDOL	MONL	677.8	5	+300	+470	+1.57
7080	7110	679.9	6	+400	+560	+1.40

Table 11

Comparison of relative ground station (GS) rates $\Delta\tau_{GS1\ GS2}^{(1)}$ measured from the multiple-pass and the simultaneous pass analysis.

Station combination		Days since Jan 1st 2009	Nr.	Relative GS rate diff. in 1×10^{-12} measured from		Ratio
GS 1	GS 2			Multiple-pass analysis	Simultaneous pass	
GO1L	MDOL	669.7	1	−5.97	−0.26	+23.23
7125	7080	697.5	2	−0.42	+0.20	−2.16
GO1L	MONL	666.6	3	−1.72	−1.88	+1.09
7125	7110	687.2	4	+5.24	−1.82	−2.88
MDOL	MONL	677.8	5	−0.31	−0.31	+1.03
7080	7110	679.9	6	−3.91	−2.37	+1.65

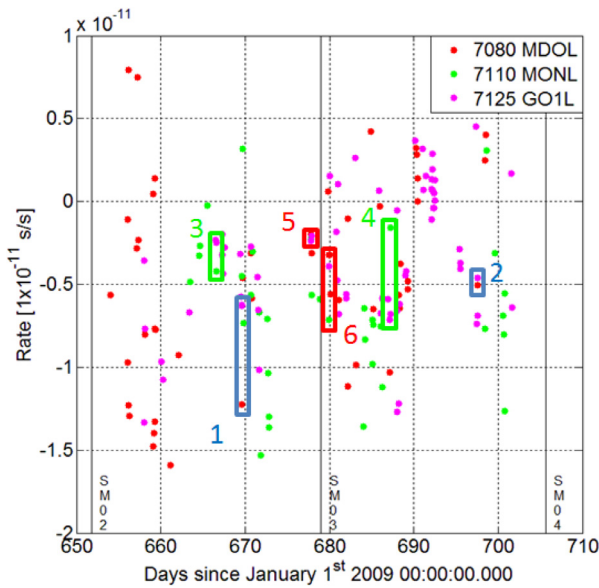


Fig. 17. Relative ground station rates $\Delta\tau_{Multi\text{-}pass\ GS1\ GS2}^{(1)}$ measured from the rate residuals with respect to the averaged trend from the multiple-pass analysis. The boxes highlight the data from two ground stations which were used to estimate the relative offset. The measured values can be found via their numbers in Table 11. (For interpretation of the references to colour in this figure legend, the reader is referred to the web version of this article.)

tween three of the ground stations. The simultaneous passes from three stations were handled like three simultaneous passes from two stations. Within the multiple-pass analysis fit we used the single passes from one station as well as all simultaneous passes from two or three stations. In order to enable a direct comparison of the two methods we only compared timing differences at simultaneous passes (common-view time transfer).

Figs. 15 and 16 show the relative offsets derived with multiple-pass and the simultaneous pass analysis respectively. Table 10 lists the values we measured for each ground station combination on two dates. Accordingly Figs. 17 and 18 show the relative rates while the measured values are listed in Table 11 similarly. The

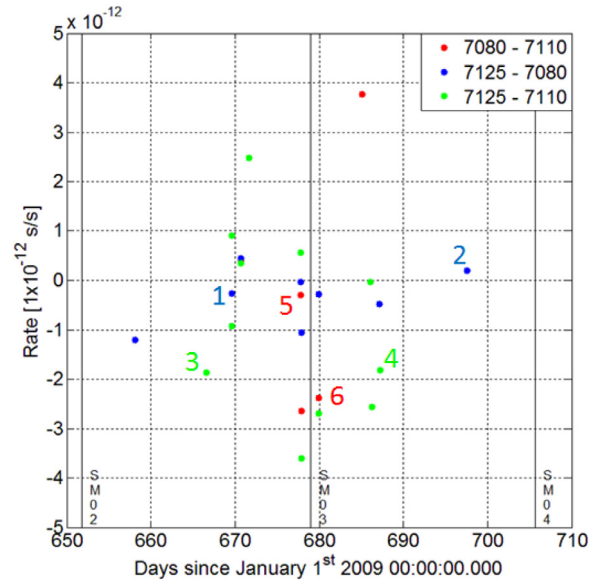


Fig. 18. Relative ground station rates $\Delta\tau_{Simu\text{-}pass\ GS1\ GS2}^{(1)}$ measured from the simultaneous passes. The measured values can be found via their numbers in Table 11. (For interpretation of the references to colour in this figure legend, the reader is referred to the web version of this article.)

passes selected for the comparison are highlighted and numbered from 1 to 6 in the figures and the tables.

During the selected timeframe we measured relative ground station clock offsets $\Delta\tau_{GS1\ GS2}^{(0)}$ between 33 ns and 560 ns (Table 10). The offsets estimated with the two approaches agree quite well for the two ground stations 7125 GO1L and 7110 MONL (Nr. 3 and 4) and less good for the station combination 7080 MDOL and 7110 MONL (Nr. 5 and 6). The station combination 7125 GO1L and 7080 MDOL showed the largest difference (Nr. 1 and 2).

We measured the relative rates $\Delta\tau_{GS1\ GS2}^{(1)}$ between the ground station clocks to values between 2×10^{-13} and 6×10^{-12} during the selected timeframe (see Table 11). The relative rates agree less good than the relative offsets because they are more sensitive to uncertainties the nominal LRO trajectory and from the corrections. The measured values basically agree with the stability values

Cash et al. (2008) reported for the timing systems that are utilized at the ground stations (see Table 1 and Table 2).

Overall simultaneous passes are more suitable for measuring the differences than the multiple-pass analysis since they are less affected by uncertainties. LRO clock and orbit errors do not affect the accuracy of the ground to ground time transfer (Sun et al., 2013b) which only leaves local differences between the ground stations, coming from their clocks and local atmospheric conditions. Thus they allow for direct ground to ground time transfer at an accuracy of at least 500 ps (LOLA timestamp accuracy). However there needs to be frequent coverage with simultaneous passes between all ground stations for continuous monitoring of their differences.

Using the closure equation on the differences derived from the simultaneous passes where three stations were ranging via

$$\Delta\tau_{7125-7110}^{(0)} - \Delta\tau_{7125-7080}^{(0)} - \Delta\tau_{7080-7110}^{(0)} = 0 \quad (24)$$

allows to further check the consistency of the estimated relative offsets. For the values estimated with the simultaneous pass analysis we saw remaining deviations of ± 0.3 ns for passes from all three stations on day 670.7, 677.8, 677.9 and 679.9 (see Fig. 16).

While the values from the multiple-pass analysis are affected by random LRO clock, correction and orbit errors, the fit provides better coverage for monitoring the station timing behavior. Even stations from different continents, which are too much separated for simultaneous ranging, could be analyzed. However due to the limited stability of the LRO clock (2×10^{-13} over 10,000 s, results in 480 ns which is ≈ 145 m over 28 days, one mission phase) the measurement of timing differences in non-common view is not very accurate since it becomes subject of too much interpretation (see Fig. 14).

In order to quantify the effect due to variations of the local atmospheric condition between the stations, we estimated the $1-\sigma$ variation of the tropospheric corrections around its mean value for all single and simultaneous passes during SM02 and SM3. Since the $1-\sigma$ variation of 8.26 ns around a mean value of 18.1 ns is smaller than the relative offsets themselves, the differences between the stations due to local atmospheric conditions are small.

8. Discussion and conclusion

International Laser Ranging Service ground stations performed one-way laser ranging to NASA's Lunar Reconnaissance Orbiter in orbit around the Moon. These measurements complement the radio and the altimetric crossover observations with an additional type of tracking data.

By using the nominal LRO trajectory, we pair and analyze the one-way laser ranging data. The paired predicted and measured receive times provide a link between the TDB and the MET time scale. We apply various corrections on both the predicted and the measured receive times. The results of our processing and analysis are affected by the random errors of the LRO clock, the completeness of the corrections and the errors of the nominal LRO trajectory. The random LRO clock errors and the errors due to the incomplete corrections affect the approximation of the LRO clock with the polynomial fits and with that the estimated LRO clock parameters. However applying fits over longer timeframes (e.g. one mission phase) allows to compensate these as well as errors from the nominal trajectory due to the averaging over time to some extent. Furthermore the accuracy of 9 m (30 ns at the arc overlaps) the nominal trajectory allows us to accurately investigate various aspects of the experiment and its components. The properly assessment of the coupling between the signature of the orbital dynamics and the clock errors would require a concurrent orbit determination and clock parameter estimation, which is outside the scope of this article. Bauer et al. (2016) analyzed such coupling in

detail while using the one-way measurements for demonstration of LRO orbit determination.

We derived ≈ 3000 hours of tracking data that feature 64 million Full Rate observations at a precision of 12.6 cm which confirms and even supersedes the LOLA timestamp accuracy of ≈ 15 cm. The averaging to Normal Points reduces this amount to 1.5 million observations with a measurement precision of only 5.6 cm and further removes the effect of ground station characteristics. Beside the experiment and the ground station performance, the statistical analysis provides information for laser ranging data simulations from a worldwide ground station network to a target beyond an Earth orbit. These information are of interest within mission analysis as carried out by Turyshev et al. (2010) and Dirkx et al. (2014 and 2015) for example.

From the analysis of single and multiple passes we derived the LRO clock parameters offset, rate, aging and its change through the mission time. By comparing the parameters from both approaches we derived estimates on their precision. Over all mission phases we estimated the rate to an overall average value of 6.9×10^{-8} and at a precision of 8.1×10^{-12} , the aging to an overall average value of 1.6×10^{-12} /day and at a precision of 1.2×10^{-12} /day and the change of the aging to an overall average value of 2.3×10^{-14} /day² and at a precision of 9.2×10^{-14} /day². We further referenced the MET to the TDB time scale, thus performing ground to space time transfer, at an accuracy of 166 ns over two and 256 ns over all mission phases. A manual data editing is thereby used to remove outliers and derive a link of good quality. Since the nominal LRO trajectory error is 30 ns, the influence of random LRO clock errors and the incomplete corrections on the referencing were larger.

Furthermore we carried out ground to ground time transfer by analyzing the residuals of different ground station passes with respect to the multiple-pass analysis fit and measuring them directly with the simultaneous pass analysis. We compare the results by measuring the differences during simultaneous passes (common-view time transfer). We measured the relative offsets to values between 33 ns and 560 ns and the relative rates between 2×10^{-13} and 6×10^{-12} . The simultaneous pass analysis provides accurate station clock differences at the LOLA timestamp precision of 500 ps since it is insensitive to orbit and LRO clock errors. Compared to the simultaneous pass analysis, the multiple-pass analysis is affected by nominal LRO trajectory errors (30 ns), random LRO clock errors and the incomplete corrections. Because of these errors the station differences from the multiple-pass analysis are less accurate if measured from simultaneous passes and unfeasible if measured from consecutive passes due to the accumulation of errors. However the multiple-pass analysis allows to monitor the station clock behavior over longer timeframes and even between stations from different continents.

While laser ranging ground stations typically measure times of flight very precise, the application of one-way data requires an accurate total referencing of the fire times. Simultaneous passes can be used to track the timing differences of the ground station clocks or for time transfer from a well referenced master station as long as there is frequent coverage with passes between all stations. Therefore the field of view of a receiver onboard a spacecraft should be wide enough, so that ranging even from widely spaced stations can occur as with the upcoming ELT experiment for example. A good strategy could be scheduling simultaneous passes between consecutive stations once around the globe in regular time intervals.

To improve the accuracy of the corrections and thus the results, the variation of the LRO clock rate due to temperature change could be incorporated within future work. Further the modeling of the atmospheric corrections could be improved by applying a continuously updated instead of just one averaged correction value if continuous meteo data is available throughout a pass.

Overall the results from the characterization of the LRO and the ground station clock differences provide information that are required for the LRO orbit determination based on one-way laser ranging data. Due to the one-way setup the LRO initial state and all involved timing systems in space and on ground have to be estimated simultaneously which introduces many correlated parameters. Applying the values from the clock characterization in form of a priori initial and covariance values allows for the estimation of all parameters as demonstrated by Bauer et al. (2016). The joint orbit determination utilizing the radio, altimetry and laser data shall enable improvement of the spacecraft positioning and the data product accuracy finally.

Acknowledgements

S. Bauer, H. Hussmann, and D. Dirx were supported by the ES-PaCE project, EC FP7 Grant Agreement 263466. Major parts of this work were carried out while the first author very much enjoyed a research visit at NASA Goddard Space Flight Center (GSFC). J.O. was hosted by MIIGAiK and supported by the Russian Science Foundation, project #14-22-00197. We thank two anonymous reviewers for their very constructive comments.

Supplementary materials

Supplementary material associated with this article can be found, in the online version, at doi:10.1016/j.icarus.2016.09.026.

References

- Bauer, S., et al., 2013. Reduction and analysis of one-way laser ranging data from ILRS ground stations to LRO. In: Proceedings of the 6th ESA International Workshop on Tracking, Telemetry and Command Systems for Space Applications, ESA-ESOC, Darmstadt, Germany, 10th–13th September.
- Bauer, S., et al., 2016. Demonstration of orbit determination for the Lunar Reconnaissance Orbiter using one-way laser ranging data. PSS 129.
- Cash, P., et al., 2008. Ultrastable oscillators for space applications. In: Proceedings of the 40th Annual Precise Time and Time Interval (PTTI) Meeting.
- Dirx, D., et al., 2014. Influence of atmospheric turbulence on planetary transceiver laser ranging. Adv. Space Res. 54 (11).
- Degnan, J., 1994. Thirty years of laser ranging. In: Proceedings of the 9th International Laser Ranging Service workshop, Canberra, Australia, 7th–11th November.
- Dirx, D., et al., 2015. Comparative analysis of one- and two-way planetary laser ranging concepts. PSS 117.
- Exertier, P., et al., 2006. Contribution of laser ranging to earth's sciences. C.R. Geosci. 338.
- Exertier, P., et al., 2011. T2L2 /J2: how to distribute the data. Ocean Surface Science Team (OSTS) Meeting, San Diego, CA, USA, 19th–21st October.
- Exertier, P., et al., 2013. T2L2: five years in space. European Frequency and Time Forum & International Frequency Control Symposium (EFTF/IFC) joint.
- Husson, V.S., 1992. Historical MOBILAS system characterization. In: Proceedings of the 8th International Laser Ranging Service workshop, Annapolis, Maryland, USA, 18th–22th May.
- International Laser Ranging Service (ILRS) Website. <<http://ilrs.gsfc.nasa.gov>> retrieved in July 2016.
- Kaplan, G.H., 2005. The IAU Resolutions on Astronomical Constants, Time Scales, and the Fundamental Reference Frame. U.S. Naval Observatory Circular No. 179.
- Lemoine, F., et al., 2014. GRGM900C: a degree 900 lunar gravity model from GRAIL primary and extended mission data. Geophys. Res. Lett. 41 (10).
- Lombardi, M.A., 2001. Fundamentals of time and frequency. published in The Mechanics Handbook. CRC Press.
- Mao, D., et al., 2011. Laser ranging status report. LOLA Meeting. Purdue University, Indiana USA.
- Mao, D., et al., 2014a. LRO orbit determination with laser ranging data. In: Proceedings of the 19th International Laser Ranging Service workshop, Annapolis, Maryland, USA, 27th–31th October.
- Mao, D., et al., 2014b. Time-transfer experiments between satellite laser ranging ground stations via one-way laser ranging to the Lunar Reconnaissance Orbiter. In: Proceedings of the 19th International Laser Ranging Service workshop, Annapolis, Maryland, USA, 27th–31th October.
- Marini, J.W., et al., 1973. Correction of Laser Range Tracking Data for Atmospheric Refraction at Elevations Above 10 Degrees. Goddard Space Flight Center NASA Report X-591-73-351.
- Mazarico, E., et al., 2012. Orbit determination of the Lunar Reconnaissance Orbiter. J. Geod. 86, 193–207.
- Mazarico, E., et al., 2013. Improved orbit determination of lunar orbiters with lunar gravity fields obtained by the GRAIL mission. In: Proceedings of the 44th Lunar and Planetary Science Conference (LPSC), Woodlands, Texas, USA, 18th–23rd March.
- McGarry, J., et al., 2011. The first ILRS laser transponder Mission: laser ranging to NASA's Lunar Reconnaissance Orbiter. In: Proceedings of the 17th International Laser Ranging workshop, Bad Koetzing Germany, 16th–20th May.
- McGarry, J., et al., 2013. LRO-LR: four years of history-making laser ranging. In: Proceedings of the 18th International Laser Ranging workshop, Fujiyoshida Japan, 11th–15th November.
- Moyer, T.D., 1971. Mathematical Formulation of the Double-Precision Orbit Determination Program (DPODP). NASA JPL CALTEC Technical Report 32-1527.
- Moyer, T.D., 1981. Transformation from proper time on earth to coordinate time in solar system barycentric space-time frame of reference part 1. Celestial Mech. 23, 33–56.
- NAIF LRO SPICE archive: Lunar Reconnaissance Orbiter SPICE archive at the NAIF node, ftp://naif.jpl.nasa.gov/pub/naif/pds/data/lro-l-spice-6-v1.0/lrosp_1000/, retrieved in July 2015.
- Neumann, G.A., et al., 2006. Laser ranging at interplanetary distances. In: Proceedings of the 15th International Laser Ranging workshop, Canberra Australia, 15th–20th October.
- Pearlman, M.R., et al., 2002. The international laser ranging service. Adv. Space Res. 30 (2), 135–143.
- Ramos-Izquierdo, L., et al., 2009. Optical system design and integration of the Lunar Orbiter Laser Altimeter. Appl. Opt. 48 (16), 3035–3049.
- Riris, H., Cavanaugh, J., Neumann, G., 2009. Calibration Document for the Lunar Orbiter Laser Altimeter (LOLA). NASA Goddard Space Flight Center. <http://imbrium.mit.edu/CALIB/CALIBRPT.PDF>.
- Rothacher, M., 2000. Vorlesungsskriptum Erdmessung und Satellitengeodäsie 2. TU München.
- Schlicht, A., et al., 2012. The European Laser Timing experiment (ELT) and data centre (ELT-DC). Mitteilung des Bundesamtes für Kartographie und Geodäsie: Proceedings of the 17th International Workshop on Laser Ranging, Vol. 48.
- Schreiber, U., et al., 2009. The European Laser Timing (ELT) experiment on-board ACES. In: Proceedings of the 23rd European Frequency and Time Forum (EFTF 2009).
- Smith, D.E., et al., 2006a. Two-Way laser link over interplanetary distance. Science 311 (53).
- Smith, D.E., et al., 2006b. Laser ranging to the Lunar Reconnaissance Orbiter (LRO). In: Proceedings of the 15th International Laser Ranging workshop, Canberra Australia, 15th–20th October.
- Sun, X., et al., 2013a. Free space laser communication experiments from earth to the Lunar Reconnaissance Orbiter in lunar orbit. Opt. Express 21 (2).
- Sun, X., et al., 2013b. Time transfer between satellite laser ranging stations via simultaneous laser ranging to the Lunar Reconnaissance Orbiter. In: Proceedings of the 18th International Laser Ranging workshop, Fujiyoshida Japan, 11th–15th November.
- Torrence, M.H., et al., 1984. The construction and testing of normal points at goddard space flight center. In: Proceedings of the 5th International Laser Ranging workshop, 10th–14th, 506. Herstmonceux, UK.
- Turyshv, S., et al., 2010. Advancing tests of relativistic gravity via laser ranging to phobos. Exper. Astron. 28, 209–249.
- Zuber, M.T., et al., 2010. The Lunar Reconnaissance Orbiter laser ranging investigation. Space Sci. Rev. 150 (1–4), 63–80.